Icarus **155**, 454–474 (2002)
doi:10.1006/icar.2001.6737, available online at http://www.idealibrary.com on IDEAL®

Stable Chaos in High-Order Jovian Resonances

Kleomenis Tsiganis, Harry Varvoglis, and John D. Hadjidemetriou

Section of Astrophysics, Astronomy, and Mechanics, Department of Physics, University of Thessaloniki, 540 06 Thessaloniki, Greece
E-mail: tsiganis@astro.auth.gr

Received February 13, 2001; revised August 7, 2001

In a previous publication (Tsiganis *et al.* 2000, *Icarus* 146, 240–252), we argued that the occurrence of *stable chaos* in the 12/7 mean motion resonance with Jupiter is related to the fact that there do not exist families of periodic orbits in the planar elliptic restricted problem and in the 3-D circular problem corresponding to this resonance. In the present paper we show that nonexistence of resonant periodic orbits, both for the planar and for the 3-D problem, also occurs in other jovian resonances—namely the 11/4, 22/9, 13/6, and 18/7—where cases of real asteroids on *stable-chaotic* orbits have been identified. This property may provide a "protection mechanism," leading to semiconfinement of chaotic orbits and extremely slow migration in the space of proper elements, so that diffusion is practically unrelated to the value of the Lyapunov time, T_L, of chaotic orbits. However, we show that, in more complicated dynamical models, the long-term evolution of chaotic orbits initiated in the vicinity of these resonances may also be governed by secular resonances. Finally, we find that stable-chaotic orbits have a characteristic spectrum of autocorrelation times: for the action conjugate to the critical argument the autocorrelation time is of the order of the Lyapunov time, while for the eccentricity- and inclination-related actions the autocorrelation time may be longer than $10^3 T_L$. This behavior is consistent with the trajectory being *sticky* around a manifold of lower-than-full dimensionality in phase space (e.g., a 4-D submanifold of the 5-D energy manifold in a three-degrees-of-freedom autonomus Hamiltonian system) and reflects the inability of these "flawed" resonances to modify secular motion significantly, at least for times of the order of 200 Myr.

Key Words: **asteroids; dynamics; celestial mechanics; chaos.**

1. INTRODUCTION

One of the most interesting, newly discovered, phenomena in Solar System dynamics is a type of asteroid motion commonly referred to as *stable chaos*. The first example, asteroid (522) Helga, was given by Milani and Nobili (1992), who used the aforementioned oxymoron to stress the apparent contradiction between the short value of the Lyapunov time,[1] $T_L \approx 7{,}000$ years, of Helga and the remarkable stability of its orbital elements, which do not change appreciably for times of the order of $10^3 T_L$. This asteroid, having proper semi-major axis $a_P \approx 3.63$ AU and proper eccentricity $e_P \approx 0.05$, is situated close to the nominal location of the 12/7 mean motion resonance of the restricted three-body problem. The authors found the corresponding critical argument, $\sigma = 7\lambda - 12\lambda_J$ (where λ denotes the mean longitude and the subscript J refers to the elements of Jupiter throughout this paper), to alternate between libration and circulation (in both senses), concluding thus that the 12/7 resonance is the mechanism responsible for chaos. The explanation, given in their paper, for the stability of Helga's orbit was a secular protection mechanism, related to the evolution of the argument $\varpi - \varpi_J$ (where ϖ is the perihelion longitude), which is mostly librating. The maximum value of the osculating eccentricity ($e \approx 0.1$) is achieved when $\varpi - \varpi_J \approx 0$ and, thus, conjunction with Jupiter occurs at perihelion and close encounters between Jupiter and Helga cannot remove this object from the resonance. Further evidence concerning stable chaos in the neighborhood of Helga was presented by Holman and Murray (1996), who integrated 10 clones of Helga for 5 Gyr, finding both late escapers (with escape times greater than 800 Myr) and surviving particles.

Subsequently, Milani *et al.* (1997) showed that asteroids in stable chaos (ASCs) are quite frequent in many places of the main asteroid belt, as well as the Trojan swarms, raising thus an important question concerning the overall stability of the ateroid belt(s). The authors concluded that the occurrence of stable chaos in the main belt must be related to medium- to high-order mean motion resonances; Dvorak and Tsiganis (2000) argue that, similarly, stable chaos in the Trojan swarms is generated by *nonlinear* secular resonances. However, not every case of stable chaos found so far can be explained by the sole action of high-order mean motion resonances. For example, the large variations of the semi-major axis of the asteroid (490) Veritas can only be explained by employing the notion of *three-body resonances* (Nesvorný and Morbidelli 1998, see also Murray *et al.* 1998) of the Jupiter-Saturn-asteroid type, defined by the relation $p\dot{\lambda}_J + q\dot{\lambda}_S + r\dot{\lambda} \simeq 0$, where p, q, and r are integers satisfying the d'Alembert rules. Šidlichovský (1999) performed a numerical integration of the orbits of the first 100 numbered asteroids,

[1] The Lyapunov time is defined as $T_L = 1/\gamma$, where γ is the Lyapunov characteristic exponent, i.e., the average rate of exponential divergence of initially close-by orbits, a standard measure for chaos.

0019-1035/02 $35.00

a large fraction of which turned out to be chaotic. Among these objects some were found to be in a mean motion resonance with Jupiter, some in a mean motion resonance with Mars, and the rest in a three-body resonance.

In a previous publication (Tsiganis *et al*. 2000, hereafter Paper I) we revisited the problem of the motion of (522) Helga. We performed a numerical integration, showing that the orbital elements of Helga remain stable for times of the order of 2 Gyr. However, integrating a group of particles with an initial phase shift with respect to Helga, we found that most particles escaped within 50 Myr, with a mean escape time of $\sim$10 Myr. The remaining particles where the ones that had initial phases in the interval $-\pi/3 \leq \varpi - \varpi_J \leq \pi/3$, and Helga resided in the border between the escaping and the surviving set. Other orbits with almost identical behavior to that of Helga were also found close to these borders. Also, the time series of the eccentricity-related Delaunay actions had correlation times that were much longer (by many orders of magnitude) than the Lyapunov time. The results were almost the same when the perturbations of all four outer planets were taken into account. This picture fits well into a *stickiness scenario*, as proposed by Murison *et al*. (1994) and Varvoglis and Anastasiadis (1996), but the clearly chaotic evolution of the critical argument $\sigma = 7\lambda - 12\lambda_J$ implies that, if the notion of stickiness is to be used, it should be extended for many-dimensional dynamical systems (for a detailed discussion see Paper I). We will come back to this point at the end of the present paper.

In Paper I, the main family of resonant periodic orbits of the 12/7 resonance, which appear as fixed points in a Poincaré section of the planar ciruclar restricted three-body problem, was studied. We found however that, contrary to several other mean motion resonances, e.g., the 2/1 and 3/1 resonances, there does not exist on this family a bifurcation point for families of periodic orbits of the elliptic problem and of the 3-D problem. This means that as soon as the orbit of Jupiter becomes elliptic, no periodic orbits at this resonance exist, and the same is true for 3-D orbits. As a consequence, the phase space at this resonance is expected to be "smooth," because the periodic orbits (or fixed points of the Poincaré map, or fixed points of the averaged Hamiltonian) typically appear in stable–unstable pairs but, in this case, no stable and unstable manifolds exist in the phase space. Since the homoclinic loops, associated with the unstable periodic orbits, are known to divide the plane ($X = e\cos(\varpi - \varpi_J)$, $Y = e\sin(\varpi - \varpi_J)$) into three, topologically distinct, regions (internal circulation, libration, and external circulation), we concluded that this is not the case in the 12/7 resonance. This in turn means that, in the three-body problem, the mechanism which in other resonances (e.g., the 3/1 case; Hadjidemetriou 1993a) was found to be responsible for the transport of chaotic orbits from low- to high-eccentricity regions of the phase space does not exist in the 12/7 mean motion resonance. Thus, the eccentricity of chaotic orbits, initiated in the vicinity of this resonance, cannot grow easily to Jupiter-crossing values. For proper eccentricities of the order of the forced eccentricity, $e_P < e_J \approx 0.048$, libration orbits exist, while for $e_P > e_J$ the argument $\varpi - \varpi_J$ is circulating. For (522) Helga, having $e_P \approx e_J$, the critical argument barely manages to circulate. This behavior, which persists even when all outer planets pertub the asteroid, can be considered as a protection mechanism, in accordance with the results of Milani and Nobili (1992). We note however that, in models containing more than one perturbing planet, the depletion of a gap corresponding to an orbital resonance is drastically enhanced by the overlap of secular resonances that are generated inside the libration zone of the orbital resonance (Moons and Morbidelli 1995). This is in fact the presently accepted mechanism for the depletion of the resonances associated with the Kirkwood gaps.

In the present paper we study the motion of asteroids in the vicinity of the 11/4, 13/6, 18/7, and 22/9 mean motion resonances, in the same spirit as in Paper I. These resonances appear to be associated with the stable-chaotic motion of the asteroids (50) Virginia, (6) Semele, (2) Pallas, and (33) Polyhymnia, respectively, according to Šidlichovský (1999). In the next section we focus on a numerical study of the long-term evolution of these four real ASCs. In Section 3 we show that all these resonances share the same property as the 12/7 resonance, namely the nonexistence of periodic orbits in the 3-D space and in the case where the orbit of Jupiter is elliptic. This is clear from the fact that there does not exist a bifurcation point on the main family of periodic orbits of the circular problem to periodic orbits either of the 3-D problem or of the elliptic problem. In Section 4 we present the results of a numerical simulation of the evolution of fictitious asteroids, initially set in the vicinity of these resonances. We show that, in a limited number of cases, the long-term evolution of these asteriods and the stability of their proper elements can change, due to the action of secular resonance, when all outer planets are taken into account. Also, we examine the properties of the autocorrelation spectra of the action time series of stable-chaotic orbits. Finally, a discussion and conclusions are given in Section 5.

2. LONG-TERM EVOLUTION OF THE REAL ASCs

First we discuss the setup of the numerical experiments presented in this study. Then we give the results concerning the long-term dynamical evolution of the four real ASCs, whose chaotic behavior can be related to a mean motion resonance with Jupiter (Šidlichovský 1999).

2.1. Numerical Setup

Two dynamical models are used throughout this paper: (i) the 3-D elliptic restricted three-body problem (hereafter 3BP) and (ii) the 3-D outer Solar System (hereafter OSS) model, in which all four outer planets are considered to interact through Newtonian gravity and perturb the massless asteroids (particles). The integrator used is the symplectic integrator of Wisdom and Holman (1991), as it is implemented in the SWIFT package

(Levison and Duncan 1994), with a time step of $\delta t = 10^{-2} T_J \approx 43$ days in all cases. In the following, the time unit will be the revolution period of Jupiter, $T_J \approx 11.86$ years. The initial conditions for the planets were taken from the Astronomical Almanac (2000) for the epoch JD 2451600.0 (2000 Feb. 26.0 TDT) and the initial conditions of the asteroids (for the same epoch) were taken from the free-access MPCORB.DAT database, provided by the Minor Planet Center (ftp://cfa-ftp.harvard.edu/pub/MPCORB/MPCORB.DAT).

2.2. Results

First, a $10^5 T_J$ integration was performed, in both models, for (2) Pallas, (33) Polyhymnia, (50) Virginia, and (86) Semele, in order to verify the results of Šidlichovský (1999) concerning the associated chaos-generating resonances and the Lyapunov time of their orbits. Then the results were extended by performing a $10^8 T_J \approx 1.2$ Gyr integration of the same objects, again in both models, to check the long-term (in)stability of their orbital elements.

In the first run ($10^5 T_J$) with the OSS model, the orbits of these asteroids turned out to be chaotic with their Lyapunov times being in the range 5,000–20,000 years, as in Šidlichovský (1999). Also, the critical arguments corresponding to the resonances, noted in the same paper, were found to alternate between libration and circulation in an erratic manner, indicating that chaos is generated by these resonances. If Jupiter is taken as the sole perturbing body,[2] the situation is somewhat different. The Lyapunov time for Pallas, Semele, and Virginia is almost the same, but the motion of Polyhymnia seems to be regular. The time evolution of the deviation vector shows a linear divergence ($\gamma \to 0 \Rightarrow T_L \to \infty$) at least for an integration spanning $\approx$10 Myr, and the critical arguments associated with the 22/9 resonance show fast circulation. Thus we conclude that, using the same set of initial conditions also in the 3BP model, "Polyhymnia" falls out of the 22/9 resonance. The quotes are used here to stress the fact that a simulation of the orbital evolution of these "asteroids" under such a simplified model (Jupiter as the sole perturbing body) is not representative of the evolution of the real objects.

The time needed for a notable change in the orbital elements of these asteroids is much longer than their Lyapunov time, as was found from a $10^8 T_J \approx 1.2$ Gyr integration. We quantify their orbital stability by computing a set of time-averaged elements (which can be considered as an approximation to *proper* elements) using a running-window averaging, similar to the one used by Morbidelli and Nesvorný (1999), of

$$X_P(t_i) = \frac{1}{N} \sum_{j=i-N/2}^{i+N/2} X(t_j), \qquad (1)$$

[2] We used the orbital elements of Jupiter at the aforementioned epoch instead of the commonly used values.

TABLE I
Averaged Elements of the Real ASCs

Asteroid	$a_P \pm \sigma(a)$	$e_P \pm \sigma(e)$	$\sin(I_P) \pm \sigma(\sin I)$
3BP model			
Virginia	2.6506 ± 0.0001	0.2540 ± 0.0010	0.0522 ± 0.0042
Pallas	2.7718 ± 0.0003	0.3198 ± 0.0036	0.5497 ± 0.0016
Polyhymnia	2.8664 ± 0.0000	0.3053 ± 0.0000	0.0399 ± 0.0003
Semele	3.1072 ± 0.0003	0.2173 ± 0.0275	0.1288 ± 0.0491
OSS model			
Virginia	—	—	—
Pallas	2.7701 ± 0.0003	0.2854 ± 0.0030	0.5475 ± 0.0003
Polyhymnia	2.8662 ± 0.0004	0.2998 ± 0.0005	0.0410 ± 0.0004
Semele	3.1062 ± 0.0009	0.1767 ± 0.0101	0.0490 ± 0.0108

where X stands for a, e, or i, and the width of the window, N, corresponds to $10^6 T_J$. Taking successive averages every $10^5 T_J$, a time series for the averaged element X_P is obtained. The stability of these orbital parameters can be visualized in Fig. 1, where a 2-D projection of the respective time series for all four asteroids (i) on the (a_P, e_P) plane and (ii) on the (a_P, i_P) plane (for both models) is shown. The mean values, $\langle X_P \rangle$, along with the respective standard deviations, as calculated from the time series of the averaged elements, can be found in Table I.

In the 3BP model the elements of Polyhymnia (22/9) are extremely stable for the whole integration time span and this is consistent with the discussion made in the previous paragraph. The elements of Virginia (11/4) are also very stable and only a slight diffusion in the space of orbital elements is detected. The situation is somewhat different for Pallas (18/7), as diffusion in eccentricity becomes apparent for times greater than $\approx$200 Myr. However, the variations Δa and Δi of its semi-major axis ($\Delta a \sim 10^{-3}$ AU) and inclination ($\Delta i \sim 0.^\circ 5$) are almost undetectable. The most unstable orbit is the one of Semele (13/6), with the maximum variation being $\Delta e \simeq 0.1$ in eccentricity and $\Delta i \simeq 8.^\circ 5$ in inclination. We note though that its elements are also quite stable for at least 200 Myr.

Although chaotic motion is expected to eventually lead to diffusion in the space of orbital elements, the time scale necessary for a notable change of the elements seems to be totally unrelated to the value of the Lyapunov time; in the "worst" case (Semele) it is longer than $10^4 T_L$. Note also that all orbits have eccentricities larger than 0.2. For Semele this means that the proximity of the 2/1 resonance cannot be neglected and, in fact, this may be the mechanism that generates diffusion both in eccentricity and inclination.

In the OSS model the results are almost the same for Polyhymnia (22/9) and Pallas (18/7) as in the 3BP model. Note though that the mean values of the averaged elements differ from those in the 3BP model. The variations of the elements of Polyhymnia are still very small, although the situation is certainly different from the 3BP case, and, surprisingly, the elements of Pallas are more stable than before. The same holds also for Semele (13/6), the variations being $\Delta e \simeq 0.03$ in eccentricity and $\Delta i \simeq 2.^\circ 5$

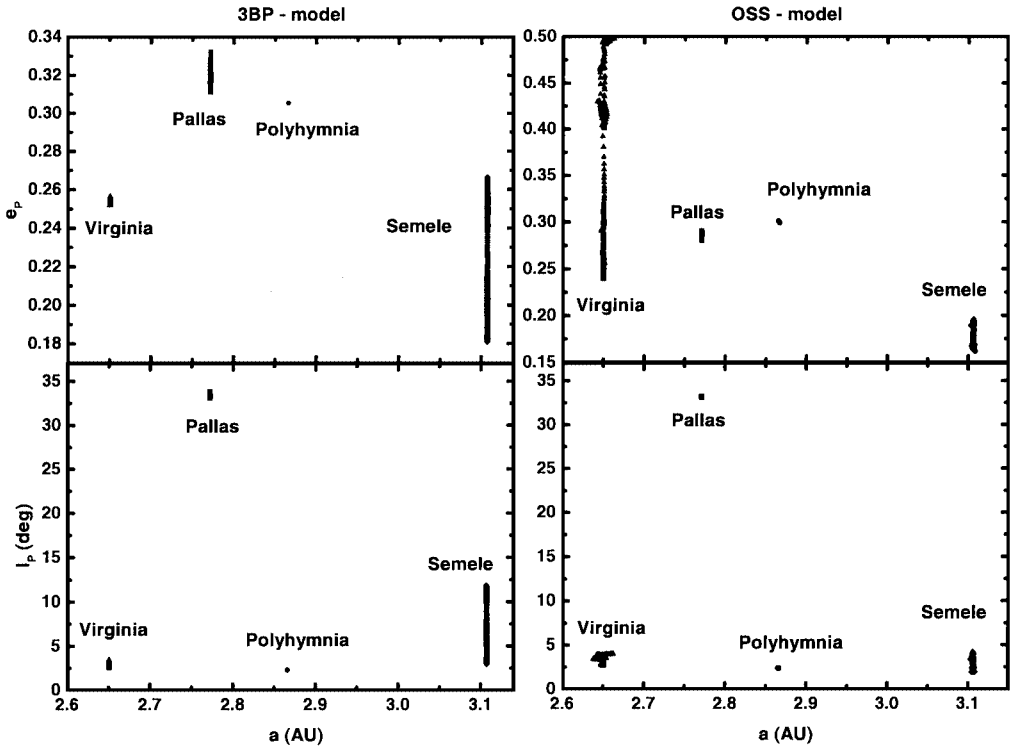

FIG. 1. A 2-D projection of the time series of the averaged elements for the four real ASCs on the (a_P, e_P) (top) and (a_P, I_P) (bottom) planes. The left frame presents the results of the 3BP model; the right frame presents those of the OSS model. The length of the time series corresponds to $\simeq 1.2 \times 10^9$ years. The names of the asteroids are marked on the figure (see text for a discussion).

in inclination. The major difference however, with respect to the 3BP model, is found for Virginia (11/4). In this integration Virginia becomes a Jupiter-crosser after $t \approx 750$ Myr and is subsequently ejected from the main belt on a hyperbolic orbit.[3] Note that the variations of its inclination are small compared to the observed eccentricity diffusion. No mean motion resonance with Jupiter of significant order (other than the 11/4) is located close to 2.65 AU. The question now is whether the resonances that have already been identified as the associated chaos-generating mechanisms are indeed the ones that force the orbits of Semele and Virginia to grow unstable.

3. DYNAMICS IN MEAN MOTION RESONANCES

The study of asteroid dynamics near mean motion resonances is usually performed in one of the following two ways: (i) construction of a suitable averaged Hamiltonian and solution of the canonical equations or (ii) computation of the location and stability character of the respective resonant periodic orbits in the nonaveraged problem. Murray and Holman (1997) used the former way to study asteroid motion in the vicinity of high-order mean motion resonances in the outer asteroid belt, while in this work we follow the latter path. A comparison between these two approaches will be given below.

We examine the phase-space structure in the vicinity of the resonances under consideration, namely the 11/4, 13/6, 18/7, and 22/9 mean motion resonances with Jupiter. First, the planar circular restricted three-body problem (hereafter *circular problem*) is considered and a study of the main family of periodic orbits in each of these resonances is performed. Then, we examine whether the corresponding families continue in (i) the planar elliptic restricted three-body problem (hereafter *elliptic problem*), where Jupiter is set to move on a fixed ellipse, and (ii) the 3-D circular restricted problem (hereafter *3-D problem*).

3.1. Circular Problem

Let us assume that Jupiter is moving on a circular orbit around the Sun and consider a uniformly rotating frame of reference, xOy, in the plane of motion, whose origin is at the center of mass of the two bodies and the x axis is on the Sun–Jupiter line. The unit of mass is the sum of the masses of the two bodies (μ is the ratio of Jupiter's mass to the total mass) and the unit of distance is the radius of Jupiter's orbit. Setting the gravitational constant $G = 1$, the period of Jupiter becomes $T_J = 2\pi$. It can be proved that in this rotating xOy frame there exist families of periodic orbits of the massless body (asteroid) that are symmetric with respect to the x axis. There are branches of families of periodic orbits for which the orbit of the asteroid is nearly circular and

[3] One always has to remember that long-time numerical integration of chaotic orbits cannot be taken as a deterministic prediction of future evolution.

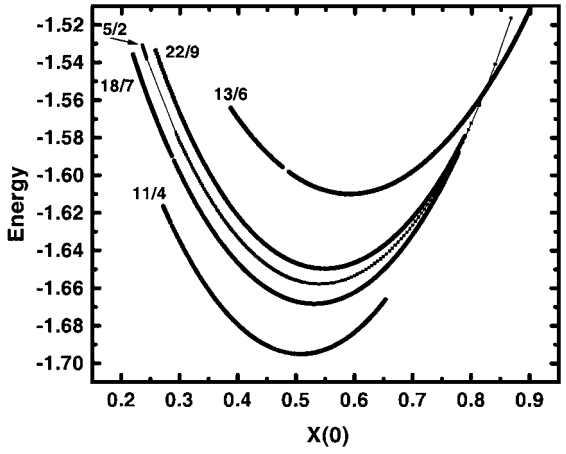

FIG. 2. The characteristic curves on the $x(0)$–energy plane of the families of periodic orbits of the resonances of the circular problem studied here. Apart from the 11/4, 18/7, 22/9, and 13/6 cases, the curve corresponding to the 5/2 resonance is shown.

branches where it is elliptic. Along a *circular branch* the eccentricity of the asteroid stays close to zero, but the semi-major axis and the mean motion varies. In contrast, along the *elliptic branch*, the eccentricity of the asteroid increases from zero to unity, while the semi-major axis and the mean motion stay almost constant. Stable and unstable orbits appear in all elliptic families. A full description is beyond the scopes of this paper and we refer to Hadjidemetriou (1993b) for a detailed discussion.

We examine here the cases $n/n' = 11/4$, 13/6, 18/7, and 22/9. At each of these resonances there exists a family of resonant periodic orbits, symmetric with respect to the x axis. Any periodic orbit of this family is uniquely determined by a point $(x(0), \dot{y}(0))$ in the x–$\dot{y}$ space (also $y(0) = 0$ and $\dot{x}(0) = 0$). Thus, a family of periodic orbits is represented by a continuous curve, called a *characteristic curve*, in the x–$\dot{y}$ space of initial conditions. Instead, we can represent a family in the x–C space, where C is the Jacobi "energy" constant. These families are shown in Fig. 2. In the same figure, we also give the characteristic curve for the 5/2 resonance, which will serve for comparison purposes. Note that, in the x–C diagram, a point does not uniquely determine an orbit, since the sign of $\dot{y}(0)$ is not indicated. Thus, the points of intersection of the characteristic curves seen in Fig. 2 do not represent the same orbit. Each family is composed of two branches: the *pericentric branch*, where the asteroid is initially at perihelion ($\varpi = 0$), and the *apocentric* branch, where the asteroid is initially at aphelion ($\varpi = \pi$). These families correspond to a specific value ($\mu \neq 0$) of Jupiter's mass.

3.2. Elliptic Problem

The dynamical evolution of an asteroid close to a resonance is determined by the topology of the phase space. This topology depends critically on the stable and unstable periodic orbits that exist, which appear as fixed points in a Poincaré surface of section. Going from the simplistic circular problem to the more complex elliptic problem, it is important to check the continuation of the families of stable and unstable periodic orbits that exist, in all cases, in the circular problem.

A family of resonant $(p + q)/p$ periodic orbits of the elliptic problem, with the eccentricity of Jupiter as a parameter, bifurcates from a point of the *elliptic branch* of the circular family, where the period is exactly equal to $T = p2\pi$. For a particular resonance, this point may or may not exist. It can be easily seen in Figs. 3–6 that this condition is *not* fulfilled in *any* of the resonances studied here (the 5/2 case is also shown in Fig. 7 for comparison); the characteristic curves of each of these resonances, in the x–T space, do not intersect the $T = p2\pi$ line. Thus, as in the case of the 12/7 resonance studied in Paper I, a homoclinic loop, which would divide the polar plane into three distinct regions and whose stochastic layer would be responsible for large-scale eccentricity transport, does not exist.

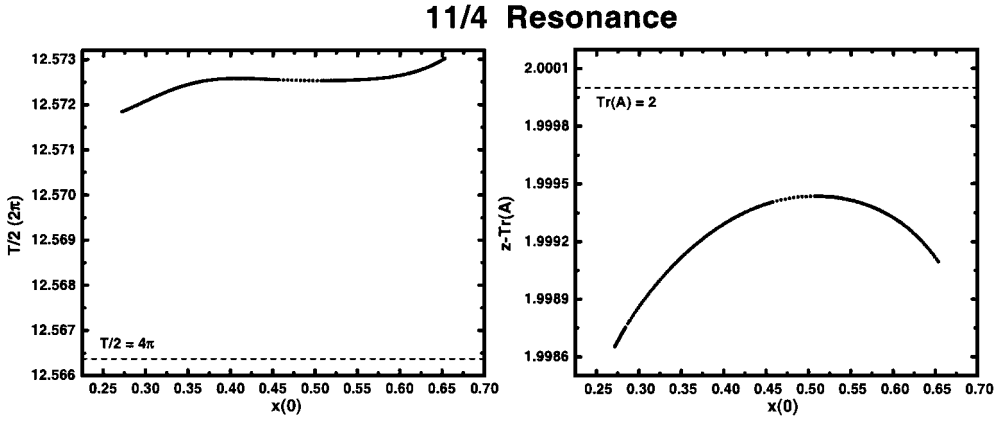

FIG. 3. (Left) The family of periodic orbits of the 11/4 resonance is plotted on the $x(0)$–$T/2$ plane (T is the period of the orbit). It is easily seen that the $T/2 = 4\pi$ line is not crossed by any periodic orbit. Thus, a bifurcation cannot occur in the elliptic problem. (Right) The trace of the monodromy matrix is plotted for each one of the periodic orbits of the circular problem. All orbits have $\mathrm{tr}(\mathbf{A}) < 2$ and no bifurcation can occur in the z direction.

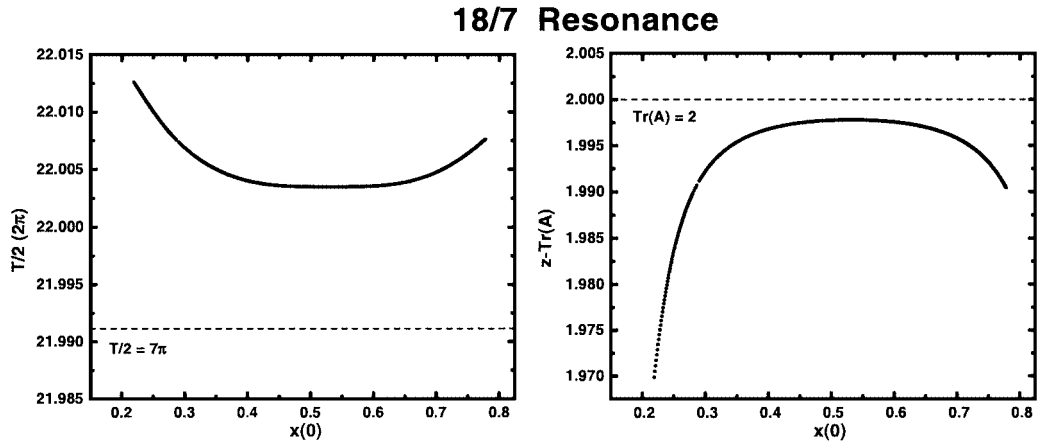

FIG. 4. The same quantities are plotted as in Fig. 3, but for the 18/7 resonance. The same comments apply also to this case.

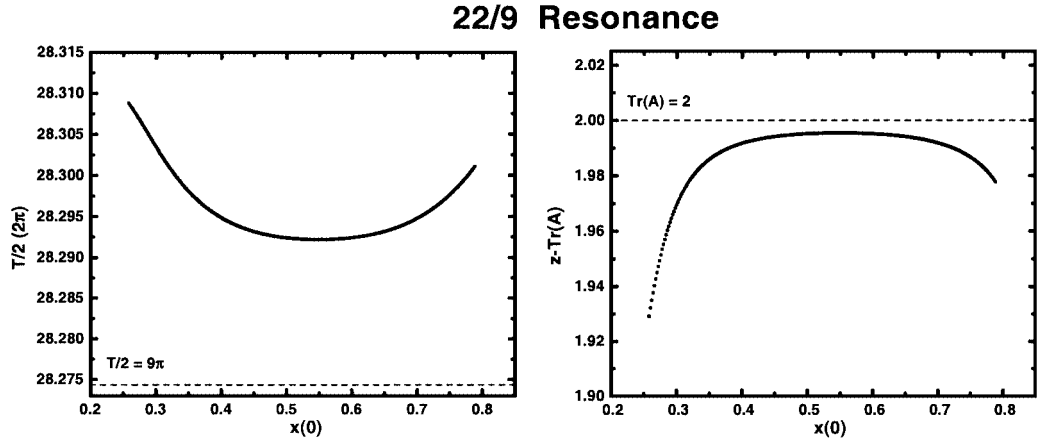

FIG. 5. The same as Figs. 3 and 4 but for the 22/9 resonance. Again, no bifurcations can occur in the elliptic or the 3-D problem.

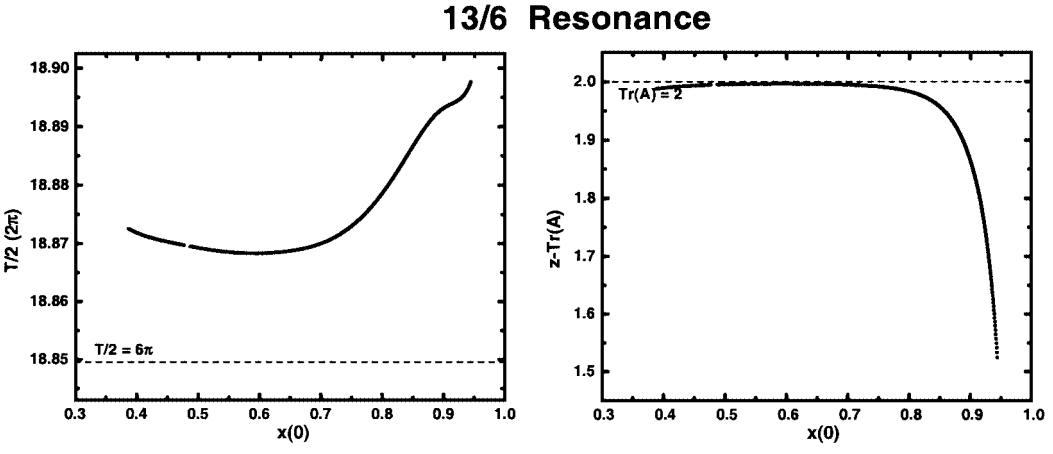

FIG. 6. The same as Figs. 3–5 but for the 13/6 resonance. Again, the conclusions about the continuation properties of the family of periodic orbits are the same. Note that tr(**A**) approaches the critical value for $0.5 < x(0) < 0.7$ but never reaches it (the calculations were performed with an accuracy of 10^{-14} in all cases).

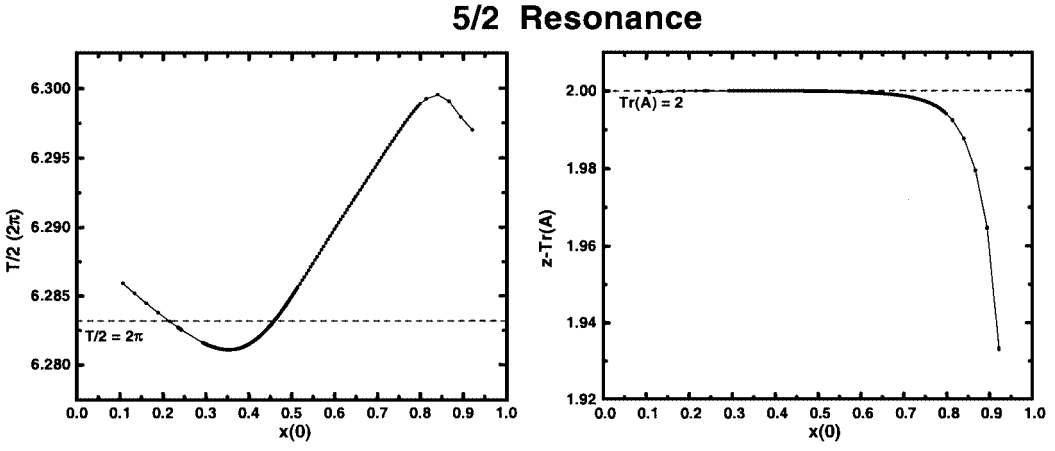

FIG. 7. The same as Figs. 3–6 but for the 5/2 resonance (shown for comparison). There are two points (values of $x(0)$) at which the period of an orbit becomes equal of 4π. These points define the eccentricity of two resonant periodic orbits of the elliptic problem. As in Fig. 6 many points approach the $\mathrm{tr}(\mathbf{A}) = 2$ line (right panel) but no bifurcation point exists for the 3-D problem.

As mentioned above, a different approach to resonant motion, in the framework of the three-body problem, consists in constructing an averaged Hamiltonian valid in the vicinity of the resonance under consideration. This is achieved by expanding the disturbing function and keeping, usually, only the lowest degree secular terms plus the cosine terms associated with this resonance (one invokes the averaging principle to get rid of the rest). For this model to be realistic, the gross topology of the phase space of the averaged problem should be as close as possible to that of the nonaveraged problem. Thus the location of the fixed points of the averaged model and their stability character should be the same as those of the periodic orbits of the nonaveraged problem. However, as discussed in Hadjidemetriou (1993b) and also in Paper I, one usually encounters the problem of "losing," misplacing, and even changing the stability character of these fixed points, through the averaging process. For example, in the case of the 3/1 resonance discussed in the following, the model of Wisdom (1983), being truncated to low degree in e, did not include the high-eccentricity fixed points. Thus, transport to $e > 0.5$ could not be predicted by this model. There are two ways to overcome this problem, namely (i) using higher degree or local expansions of the disturbing function or (ii) adding a correction term to the averaged Hamiltonian. Klafke *et al.* (1992), using the former way, and Hadjidemetriou (1993a), using the latter, recovered the high-eccentricity fixed points of the 3/1 resonance. The difference turned out to be significant as transport to $e \approx 0.9$ can explain the existence of the Sun-grazing 3/1 escapers that was noted by Farinella *et al.* (1994).

In order to appreciate the action of the unstable resonant periodic orbits and their connection to large-scale transport, we show an example for the 3/1 resonance in Fig. 8. This figure was computed using the corrected averaged model introduced by Hadjidemetriou (1993a). In both panels one can see two pairs of equilibria, each pair consisting of one stable and one unstable fixed point. These fixed points are the intersections of two stable and two unstable families of 3/1 resonant periodic orbits with the considered energy surface, $\mathcal{H} = \text{const}$. There are two low-eccentricity fixed points (stable at $\varpi - \varpi_J = 0$ and unstable at $\varpi - \varpi_J = \pi$) and two high-eccentricity fixed points (stable at $\varpi - \varpi_J = \pi$ and unstable at $\varpi - \varpi_J = 0$). As can be seen in the left panel, small-eccentricity chaotic orbits can be transported to $e \sim 0.4$ (in this system of polar coordinates e is the distance from the center), by entering the chaotic layer associated with the homoclinic orbit around the small-eccentricity fixed point. In fact it is the island of libration, around which the trajectory wanders, that leads to this eccentricity increase, within a short time scale (half the secular libration period). The same picture holds also for orbits starting in the vicinity of the high-eccentricity fixed point. For this value of $\mathcal{H}$, however, the two chaotic layers are disconnected. For higher values of $\mathcal{H}$ (see right panel) an heteroclinic intersection can cause an initially low-eccentricity orbit to "jump" to much higher values of $e \sim 0.9$ by wandering, first, around the libration island of the low-eccentricity fixed point and, afterward, around the libration island of the high-eccentricity fixed point. It is easy to imagine that the absence of a libration island and the associated homoclinic layer, i.e., the absence of resonant periodic orbits, implies that such a rapid growth of the eccentricity cannot take place.

An important element of resonant dynamics in the elliptic problem are the so-called secondary resonances, i.e., commensurabilities between the critical argument, σ, and the longitude of pericenter, $\phi = \varpi - \varpi_J$, in the averaged problem, of the form $\dot{\sigma} + k\dot{\phi} \approx 0$. The respective cosine terms appear explicitly in the expansion of the disturbing function of the elliptic problem, forming the "resonance-multiplet." The width in a of each term of the multiplet with $k \neq 0$ is also a function of Jupiter's eccentricity. If we study each term separately (this implies a second averaging), it creates a pendulum-like picture in phase

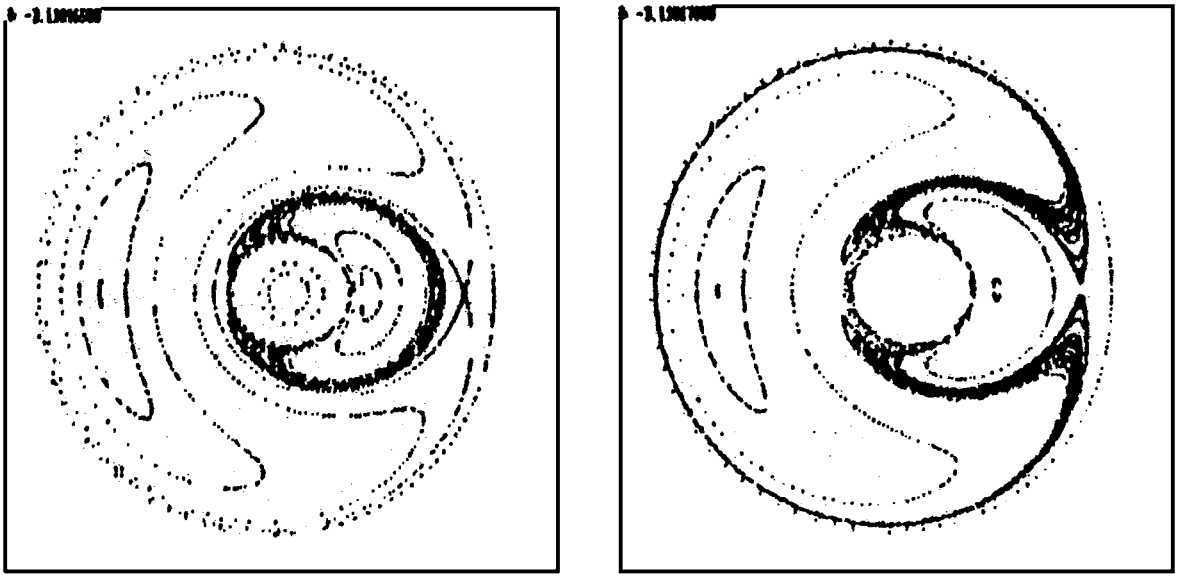

FIG. 8. The phase space in the vicinity of the 3/1 resonance (from Hadjidemetriou 1993a). The coordinates are $e\cos(\varpi - \varpi_J)$, $e\sin(\varpi - \varpi_J)$. In the left panel one sees the homoclinic loop encircling the island of libration (centered at $\varpi - \varpi_J = 0$) of the low-eccentricity periodic orbit, which drives chaotic orbits up to $e \approx 0.4$ (Mars-crossing values) within half the secular libration period. The effect of heteroclinic intersections with the high-eccentricity resonance is seen in the right panel (taken for a different energy value), where wandering around the large libration island (centered at $\varpi - \varpi_J = \pi$) leads to large-scale transport in eccentricity, up to $e \sim 0.9$ (Sun-grazers).

space. Their central fixed points are located at a different value of $a = a_k$. These fixed points correspond to periodic orbits of the averaged problem and to 2-D tori of the three-degrees-of-freedom (planar) nonaveraged problem. Murray and Holman (1997) applied Chirikov's criterion and showed that overlapping of these resonances can produce large-scale chaos, resulting in a "random-walk" behavior of a and an associated "random-walk" in e. Their analytic results fitted numerical data very well in most of the resonances they studied in the outer belt. We emphasize that this model for chaos does not depend upon the existence of resonant periodic orbits of the nonaveraged problem. In fact the absence of resonant periodic orbits, for which both σ and ϕ are stationary, is a condition for this model to be valid, as it ensures that no mechanism for fast eccentricity growth exists. In this respect the chaos found in the resonances studied in the present paper should be attributed to the overlap of the multiplet terms. The question now is how efficient this resonance-overlap is for our inner-belt commensurabilities. If a connected chaotic region that covers a wide eccentricity range (up to Jupiter-crossing values of e) is formed, then chaotic orbits will diffuse away. This diffusion can be quite slow, depending on the order of the resonance, the distance from Jupiter, and the initial value of the eccentricity, in accordance with Murray and Holman (1997). If, on the other hand, the overlap is not so exhaustive, then there can be a set of chaotic trajectories restricted within thin layers of the phase space for which large-scale transport should not be expected within a reasonably short time scale. We believe that this is the situation that one should refer to as *stable chaos*. Murray and Holman (1997) also discussed the possibility of existence of barriers to transport in phase space, but their calculations show that, if they exist, they form a set of negligible measure in the resonances they studied.

3.3. 3-D Problem

The above analysis is restricted to coplanar orbits. A more complete analysis of the dynamics requires the study of the continuation of the families of periodic orbits in a 3-D configuration space. This is done by adding the z component to the equations of motion and computing, for each one of the periodic orbits of the 2-D problem, the trace of the monodromy matrix, $\mathbf{A}$, for infinitesimally small displacements along the z direction. The periodic orbit is then said to be vertically stable if the trace of the monodromy matrix, $\mathrm{tr}(\mathbf{A})$, is absolutely smaller than 2; otherwise it is unstable. The periodic orbits for which $\mathrm{tr}(\mathbf{A}) = \pm 2$ are the vertical critical orbits from which a family of periodic orbits bifurcates to the 3-D space. Checking the vertical stability of the periodic orbits in each family (see Figs. 3–6), we found that *no* periodic orbit can bifurcate in the z direction. Thus, there are no periodic orbits in the 3-D circular problem for any of the above four resonances. This result also implies that large-scale instabilities cannot be driven by inclination variations.

3.4. Summary

According to the results presented in this section, the most efficient mechanism (in terms of amplitude modulation vs the

associated time scale) for eccentricity growth in three-body models, i.e., resonant periodic orbits, does not exist in the resonances under study. There are now two ways an asteroid on a chaotic orbit can follow to reach a planet-crossing value of e. If the overlap condition is met for the terms of the resonant multiplet, a slow eccentricity diffusion typically occurs. If resonance-overlap is not so efficient, there will be a set of confined chaotic orbits for which the only way to diffuse in action space is through *Arnol'd diffusion*. Of course the time scales involved may be longer than the age of the Universe. We believe that one should differentiate between these two types of motion. The former one is a kind of "slow chaos," quantitatively described by the model of Murray and Holman (1997), while the latter one is the behavior for which we believe that the terminology *stable chaos* is most appropriate. In the following section we are going to present numerical results that support this claim.

The situation may change if more than one perturbing planet is included in the model. The precession of Jupiter's orbit, induced by its interaction with the other planets, results in the "pulsation" of mean motion resonances. Also, secular resonances can come into play. Note, however, that no first-order (linear) secular resonance is located near the mean motion commensurabilities studied in this paper (see Knežević *et al*. 1991), at least for low inclinations ($i < 15^\circ$). Of course, we cannot know *a priori* whether the mean motion resonance can force the perihelion or nodal frequency to vary so much that a low-order secular resonance occurs inside the mean motion one, although these high-order resonances are probably too weak to do so. An analytic study of asteroid motion in this framework is beyond the purpose of the present paper. Finally, for high values of the eccentricity, the possibility of resonance-overlap between adjacent mean motion resonances cannot be neglected, although the 13/6 is the only case which is close to a low-order resonance (the 2/1).

4. LONG-TERM EVOLUTION OF FICTITIOUS ASTEROIDS

To verify the results presented above and to understand the behavior of *stable-chaotic* orbits, we performed a numerical experiment. The evolution of a group of fictitious asteroids was studied, in the frame of both the 3BP model and the OSS model.

We initially set 20 particles in the vicinity of each of the four resonances studied. Each group of 20 particles is set on a 5×4 regular grid in the (e, i) space, with $0.05 < e < 0.25$ and $5^\circ < i < 20^\circ$, while the semi-major axis, a, and the three angles, Ω, ω, and M, are set equal to those of the real ASC belonging to the respective resonance. The integration technique and the parameters used are the same as the ones in Section 2 and the total integration time was set to $10^7 T_\mathrm{J} \approx$ 120 Myr, unless some particle encountered Jupiter within a distance equal to Hill's radius, whence it was considered as "ejected."

TABLE II
Percentage of Orbits Affected by Resonance in the OSS Model

Group	Type A (%)	Type B (%)	$r_\mathrm{L}(t)$ (%) decaying
18/7	10	65	65
22/9	0	25	60
11/4	70	30	100
13/6	30	15	85

This initial configuration does not guarantee that the whole group will be initially inside the libration zone of the resonance. Two criteria were used to identify those orbits that are affected by the resonance. In the beginning, a short-time ($2 \times 10^4 T_\mathrm{J}$ years) integration was performed and the critical argument

$$\sigma = (p+q)\lambda_\mathrm{J} - p\lambda - q\varpi, \tag{2}$$

which corresponds to the resonance of the circular problem, was monitored. Those orbits, for which the critical argument librates or alternates chaotically between libration and circulation, were labeled as Type-A orbits, while those lying close to the libration zone, for which the argument is slowly circulating, were labeled as Type-B orbits. The percentages of Type-A and -B orbits differ for each resonance and for each of the two models studied; the exact numbers for the OSS model can be found in Table II. The percentage of orbits initially in resonance is appreciable for the 11/4 and 13/6 cases. Recall that the effective width in semi-major axis of a qth-order resonance is proportional to e^q and for $q = 11$ (18/7) and $q = 13$ (22/9) it should be extremely small, making it difficult to plan an initial configuration of in-resonance particles. We did not examine any of the other critical arguments associated with the resonances studied here. By processing the output of the long-term integration, we found a larger number of particles that were actually affected by the resonance than the one determined initially by the behavior of σ. The new criterion used was the exponential decay of the *autocorrelation function* of the semi-major axis time series (see Section 4.3). For the OSS model the difference between the population of predetermined resonant orbits and the ones found by processing the output is larger (see also Table II). The set of orbits that comply with the second criterion includes all Type-A orbits, the vast majority of Type-B orbits, as well as other orbits that did not seem to be affected by resonance in the short-term integration.

4.1. Stability of Mean Elements

Performing the average (see Eq. (1)) in the orbital elements, as in the case of the real ASCs, we found that the trajectories of most of the particles show a remarkable stability with time. If we define the time series of the averaged elements by Eq. (1), we may use the *mean value*, $\langle X_\mathrm{P} \rangle$, and the magnitude of its *standard*

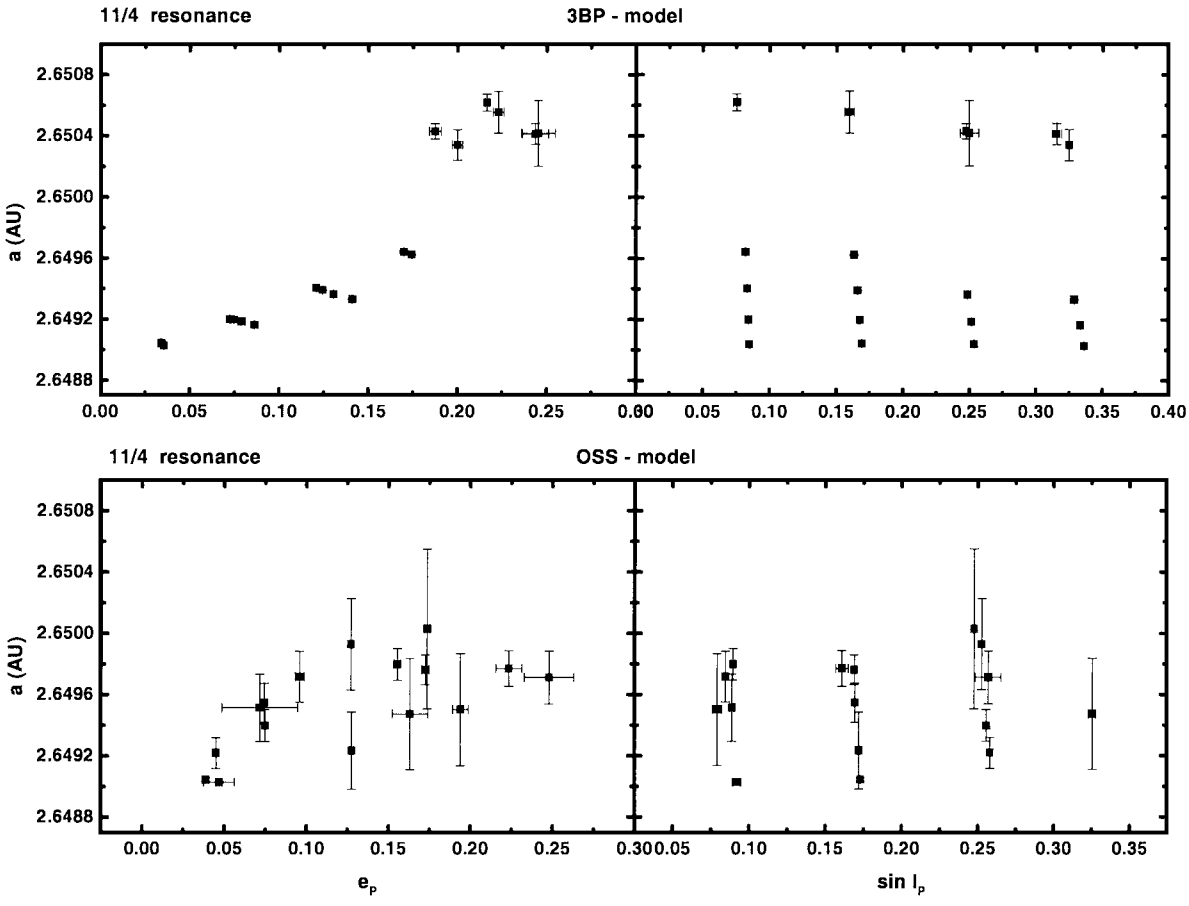

FIG. 9. The mean values of the averaged elements (squares), along with the corresponding error bars, are plotted on the planes (e_P, a_P) (left) (sin I_P, a_P) (right). All orbits started in the vicinity of the 11/4 resonance are shown except for the four escapers in the OSS integration (see text). The top panels show the results of the 3BP model, while the bottom panels are for the OSS model. The results are discussed in the text.

deviation,

$$\sigma(X_P) = \sqrt{\sum_{i=1}^{M} \frac{(X_P(t_i) - \langle X_P \rangle)^2}{M}}, \qquad (3)$$

where M is the number of windows used to cover the initial time series of the osculating elements, to quantify orbital stability. Let us now review the results for each of the four groups/resonances separately.

4.1.1. The 11/4 Region

The coordinates of each point in Fig. 9 are the $\langle X_P \rangle$ values of each particle (in the respective axes), while the length of the error bars is equal to $\sigma(X_P)$. In the 3BP model, 80% of the particles show extremely small variations of the averaged elements, with typical values for $\sigma(X_P)$ of order $\sigma(a) \sim 2 \times 10^{-6}$ AU, $\sigma(e) \sim 2 \times 10^{-5}$, and $\sigma(\sin I) \sim 5 \times 10^{-6}$. The rest of the particles (20%), having initially $e \geq 0.2$, show larger variations, with the maximum values of the standard deviations being $\sigma(a) = 0.002$ AU, $\sigma(e) = 0.01$, and $\sigma(\sin I) = 0.007$. In the frame of the OSS model, the situation is different, as one can derive from the size of the error bars in Fig. 9 (bottom panel). The majority of the particles (70%), regardless of their initial eccentricity, have standard deviations with values $\sigma(a) \sim 0.0003$ AU, $0.005 < \sigma(e) < 0.02$, and $0.001 < \sigma(\sin I) < 0.008$. Only two particles (10%) have standard deviations about one order of magnitude smaller than these typical values. Finally, four escapes (20%) were recorded (not shown in Fig. 9), with initial inclination $i = 20^\circ$ and eccentricities $e = 0.05$, 0.1, 0.15, and 0.25. The escape times were 12.4, 22.9, 105.8, and 55.9 Myr, respectively. However, the mechanism that leads these particles to escape is not the 11/4 mean motion resonance, as will be shown in Section 4.2.

4.1.2. The 18/7 Region

Figure 10 is the counterpart of Fig. 9 for the group of particles started in the vicinity of the 18/7 resonance. We can see that the variations of the averaged elements are again very small for the vast majority of the particles (90%) in the 3BP model, with typical values for the standard deviations being $\sigma(a) \sim$

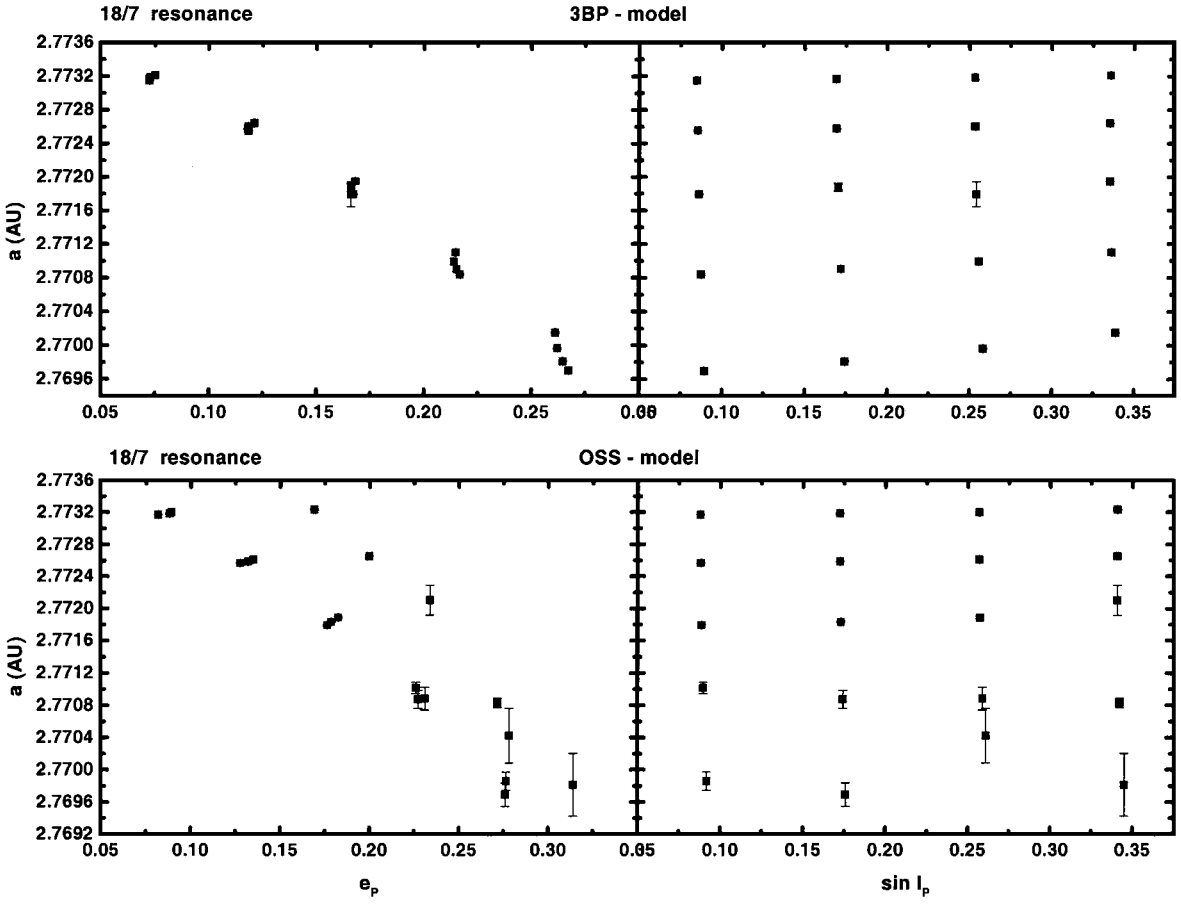

FIG. 10. The same as Fig. 8 but for the particles starting in the vicinity of the 18/7 resonance, where (2) Pallas is located.

3×10^{-6} AU, $\sigma(e) \sim 2 \times 10^{-5}$, and $\sigma(\sin I) \sim 8 \times 10^{-6}$. The remaining two cases (10%), with $e = 0.15$ initially, have $\sigma(a) \sim 10^{-4}$ AU, $\sigma(e) \sim 10^{-4}$, and $\sigma(\sin I) \sim 10^{-5}$. In the OSS model, the variations tend to become larger, although they are still very small. For initial eccentricities $e \leq 0.15$ and inclinations $i \leq 15^\circ$, the standard deviations have values $\sigma(a) \sim 5 \times 10^{-6}$ AU, $\sigma(e) \sim 10^{-4}$, and $\sigma(\sin I) \sim 2 \times 10^{-5}$. For higher values of the initial eccentricity the above values are higher and also tend to increase with increasing inclination. The typical values become $\sigma(a) \sim 2 \times 10^{-4}$ AU; $\sigma(e) \sim 4 \times 10^{-4}$ (with some cases at $e = 0.25$ reaching up to $\sigma(e) \sim 0.0013$), and $\sigma(\sin I) \sim 2 \times 10^{-4}$.

4.1.3. The 22/9 Region

The situation for the particles that start close to the 22/9 resonance (Fig. 11) is even less exciting than the 18/7 case. In the 3BP model, all particles have $\sigma(a) \sim 10^{-6}$ AU, $\sigma(e) \sim 10^{-5}$, and $\sigma(\sin I) \sim 5 \times 10^{-6}$. In the OSS model, these values become $\sigma(a) \sim 2 \times 10^{-5}$ AU, $\sigma(e) \sim 4 \times 10^{-5}$, and $\sigma(\sin I) \sim 3 \times 10^{-5}$ (for 90% of the particles), which are still extremely small. These values are the smallest found among the four resonances studied, indicating that this is the most stable region. Only two cases (initially at $i = 15^\circ$ and $e = 0.2$, 0.25), with larger values of the standard deviations, namely $\sigma(a) \sim 2 \times 10^{-4}$ AU, $\sigma(e) \sim 0.01$, and $\sigma(\sin I) \sim 0.001$, are found.

4.1.4. The 13/6 Region

Again the results are presented graphically, in Fig. 12. In the 3BP model, particles that start with $e \leq 0.15$ (and regardless of their initial inclination) have $\sigma(a) \sim 2 \times 10^{-6}$ AU, $\sigma(e) \sim 8 \times 10^{-6}$, and $\sigma(\sin I) \sim 5 \times 10^{-6}$. For larger initial eccentricities we find $\sigma(a) \sim 2 \times 10^{-4}$ AU, $\sigma(e) \sim 0.004$, and $\sigma(\sin I) \sim 0.005$. In the OSS model, the group shows again different behavior between the small- and large-eccentricity particles. For initial $e \leq 0.15$, the standard deviations are $10^{-5} < \sigma(a) < 10^{-4}$ AU, $\sigma(e) \sim 3 \times 10^{-4}$, and $\sigma(\sin I) \sim 5 \times 10^{-5}$. For $e \geq 0.2$ the variations become rather significant, with typical values of $\sigma(a) \geq 0.001$ AU, $\sigma(e) \sim 0.01$, and $\sigma(\sin I) \sim 0.008$. This value of $\sigma(a)$ is the largest one among all cases studied in this numerical experiment. The $\sigma(e)$ and $\sigma(\sin I)$ values are also the largest ones, together with those measured in the 11/4 region (OSS model).

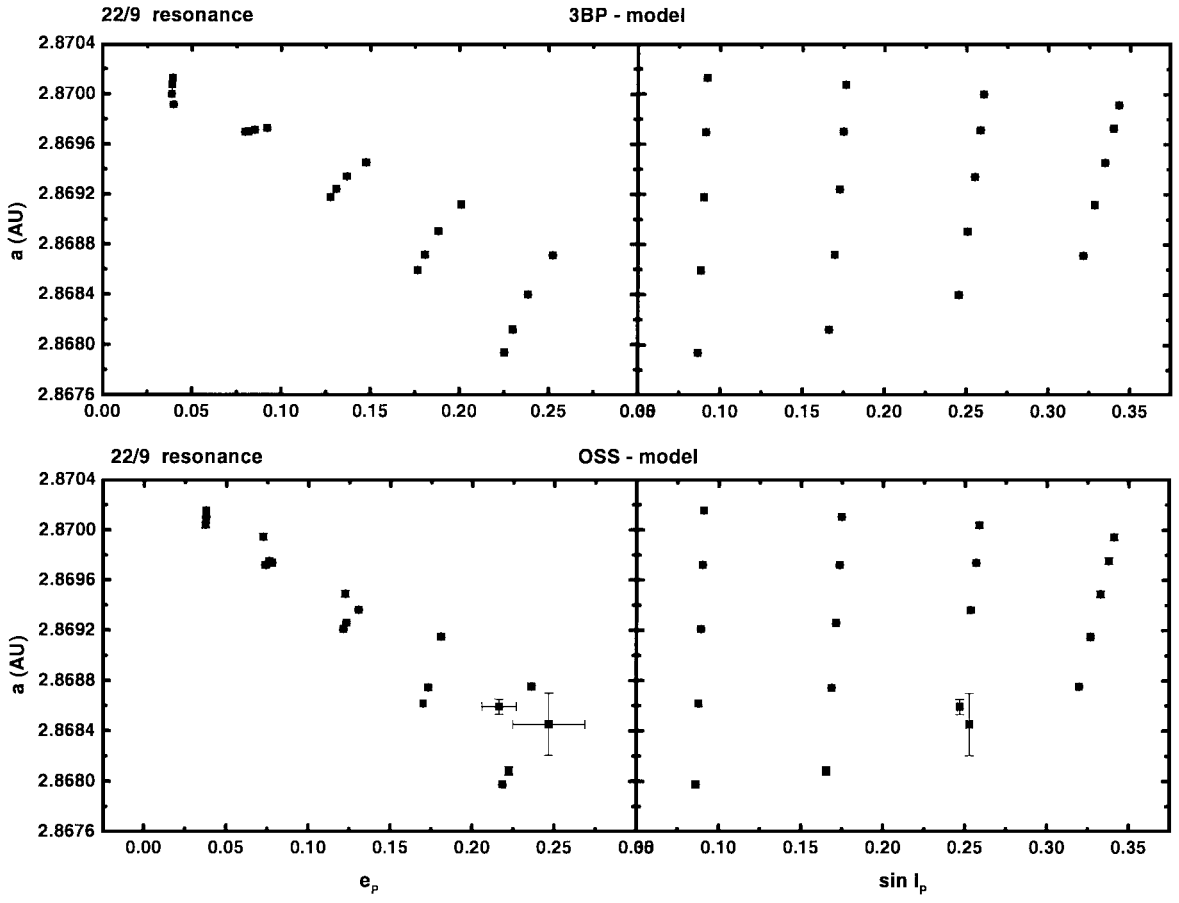

FIG. 11. The same as Figs. 8 and 9 but for the group of particles starting close of the 22/9 resonance. This is the most "stable" region of the ones studied here.

4.1.5. Summary

These results clearly demonstrate the stability of the orbits of the integrated particles, at least for times of the order of 120 Myr. Although this would be expected for orbits that were, initially, out of resonance (at least in the 3BP case), it also holds for the chaotic orbits, for which $T_L \sim 10^4$ years. Moreover, the differences between the 3BP and the OSS models are not significant, with the exception of the high-inclination ($i > 20^\circ$) part of the 11/4 region ($a \sim 2.65$ AU). Note also that the high-eccentricity part of the 13/6 region shows typically larger variations in semimajor axis than the rest of the cases. This can be understood in terms of the close proximity of mean motion (jovian and three-body) resonances at $a > 3$ AU.

4.2. The Role of Secular Resonances

Let us now treat separately the four 11/4-escapers found in the OSS integration. We note that, in the initial short-time integration, all these particles were found to follow Type-A orbits and, in particular, the critical argument $\sigma = 11\lambda_J - 4\lambda - 7\varpi$ was found to alternate chaotically between libration and circulation. However, the 11/4 resonance cannot account for the variations in e and i that lead to escape. This remark, which supports the theoretical reasoning described in Section 2 and the difference of the numerical results for this resonance between the two models, can be understood by the results shown in Figs. 13 and 14.

We examined a list of permissible combinations of secular arguments that could be resonant and, therefore, explain the eccentricity variations of these orbits. The combinations tested are the ones that Nobili *et al.* (1989) found in the *LONGSTOP1B* integration to be the highest amplitude modes of planetary precession (see Tables 4 and 5 of their paper). The values of the secular frequencies were taken from Laskar (1990) and the initial proper phases (at $t = 0$) were taken from Bretagnon (1974). A large number of overlapping pericentric secular resonances were found to govern the evolution of high-inclination orbits at $a \simeq 2.65$ AU, a picture similar to that found by Dvorak and Tsiganis (2000) in the Trojan swarms (but for nodal resonances). Most of these resonances are *nonlinear* (i.e., the corresponding critical arguments involve more than one planetary argument)

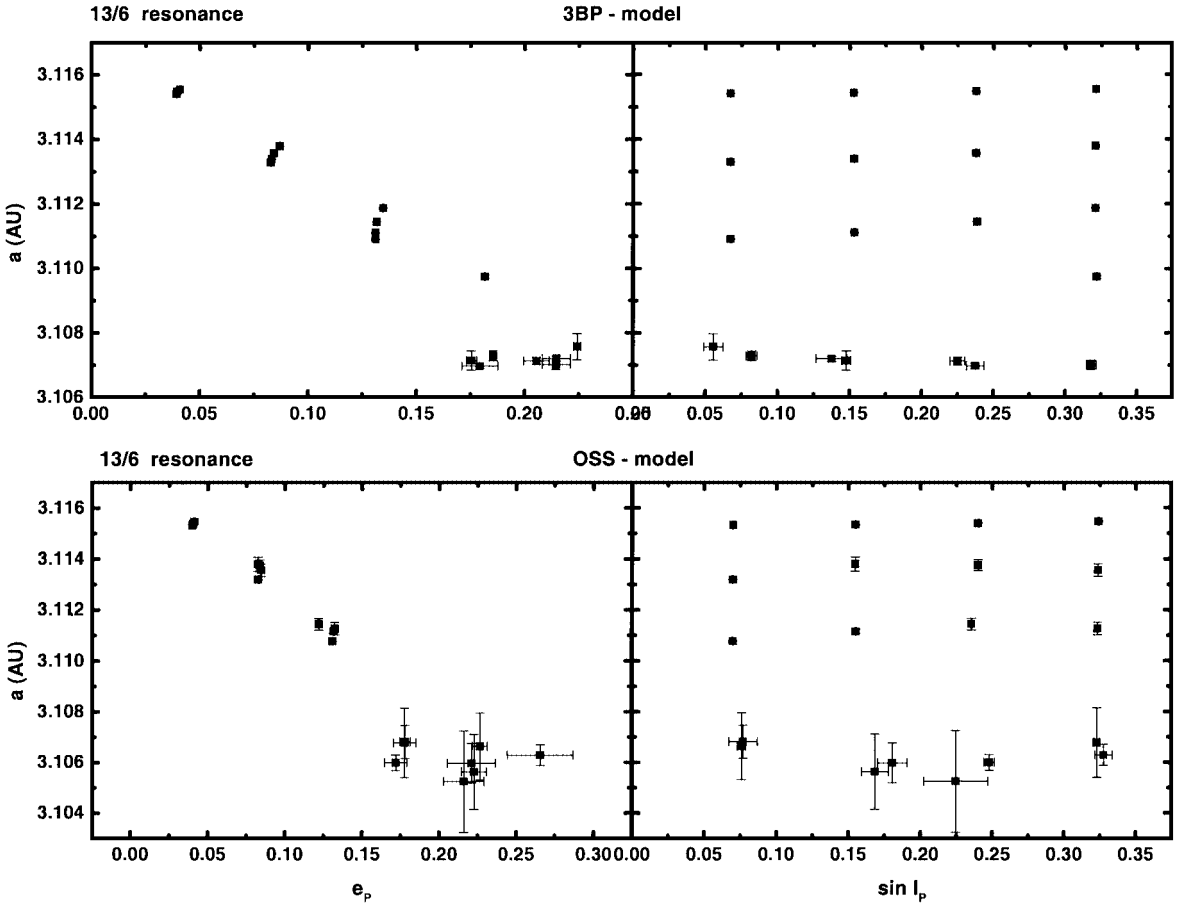

FIG. 12. The same as Figs. 8–10 but for the 13/6 group of particles. The variations become visible for $e > 0.15$.

and have periods in the range 40,000–52,000 years. However, the most important one for the evolution of these orbits turns out to be the ν_6 resonance, which is ultimately responsible for the escape. The corresponding critical argument, $\varpi - \varpi_S$, is seen in both cases (Figs. 13 and 14) to change from libration to circulation in an erratic manner. Two other arguments (one for each case) are also shown in these figures. The fact that many arguments show similar behavior at the same time indicates that the corresponding resonances overlap. Thus, in realistic models, the dynamical evolution of stable-chaotic orbits may change with time, owing to secular resonances that do not occur in simple three-body models.

We note here that the pattern of variations of the semi-major axis indicates possible action of three-body mean motion resonances, something that one also has to expect in complicated many-body models (especially close to $a \simeq 3$ AU; see Morbidelli and Nesvorný 1999), and this may contribute to a "drifting" of the trajectory in the orbital elements' space. Unfortunately no direct evidence, in terms of critical arguments, can be presented here, due to technical difficulties resulting from the "strategy" of our integration (large output interval, not saving all the elements for Saturn, etc.).

4.3. Long-Time Correlations

In Paper I we showed that one of the properties of stable chaos in the 12/7 resonance is long-time correlated motion, as it appears in the evolution of the eccentricity- and inclination-related Delaunay "actions,"[4]

$$G = \sqrt{a(1-e^2)}, \quad H = G\cos i. \tag{4}$$

This means that the autocorrelation time,[5] τ_c, of the above time series is much longer than the Lyapunov time. Recall that the amplitude of the autocorrelation function, $r(t)$, of a quasi-periodic time series varies also quasi-periodically between the values ± 1. For chaotic motion (more generally, for a stochastic process),

[4] The word "action" is commonly misused by many authors to denote the quantities that constitute the actions of the integrable problem, i.e., the Kepler problem.

[5] The autocorrelation time, τ_c, of a discrete time series is defined as the time at which the magnitude of the autocorrelation function, $r(t)$, becomes smaller that $1/e \approx 0.368$ *without increasing again*.

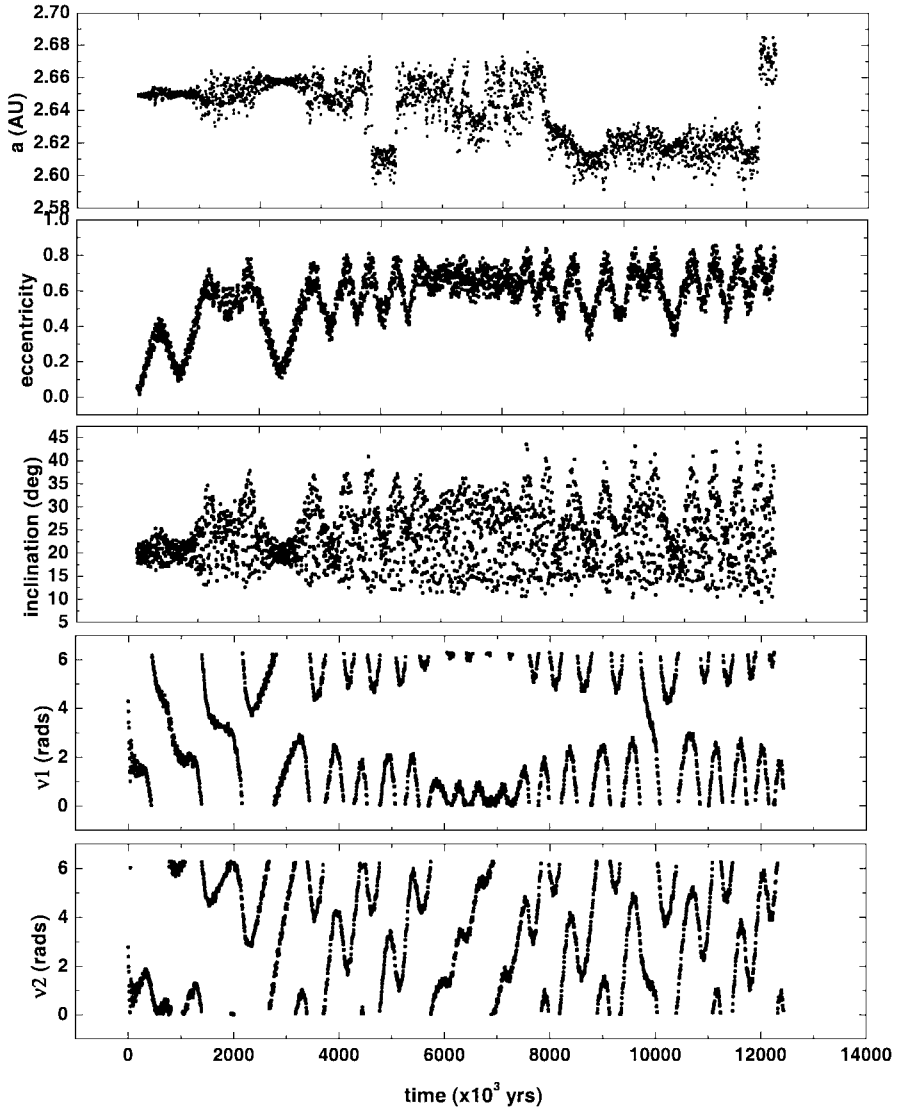

FIG. 13. Time evolution of the 11/4-escaping orbit starting at $e = 0.05, i = 20^\circ$. The osculating semi-major axis (top), eccentricity, and inclination are shown. The bottom two panels show the critical arguments corresponding to the ν_6 resonance (noted as $\nu 1$ in the figure), defined by $\langle \dot{\varpi} \rangle \approx g_6$, and the $\langle \dot{\varpi} \rangle \approx -g_5 + g_6 + g_7$ (bottom) nonlinear secular resonance (noted by $\nu 2$). These two secular resonances seem to overlap. Note the correlation between the librations of the ν_6 critical argument and the eccentricity variations.

on the other hand, $r(t)$ should decay exponentially with time. One would expect that the autocorrelation time would be of the order of $T_{\rm L}$. This, however, may not hold for all the actions. For (522) Helga we have shown that, although $\tau_{\rm c}(L)$ for $L = \sqrt{a}$ (the action conjugate to the mean longitude, λ) is of the order of $T_{\rm L} \sim 10^4$ years, the e-folding time of the $G(t)$ and $H(t)$ time series is longer than $10^3 T_{\rm L}$.

It turns out that this property is, indeed, common to all cases of stable chaos found in the present study too. We computed the $\tau_{\rm c}$s of all three actions for every orbit in the OSS model, using the records of the first $10^5 T_{\rm J} \approx 12$ Myr. Some typical $r(t)$ series, representative of the different types of behavior found, are shown in Fig. 15. We concentrate on the set of orbits for which $r_{\rm L}(t)$ (the autocorrelation function of the L time series) shows a decaying behavior with time; this property implies that the motion is chaotic. Most of these orbits show the following characteristic: $r_{\rm L}(t)$ decays exponentially with time on a relatively short time scale, while the autocorrelation functions of the G and H time series vary almost quasi-periodically, with the maximum amplitude being almost constant with time. In this respect, these orbits show exactly the same behavior as Helga's. For the escapers, on the other hand, all $r(t)$ series decay exponentially with time, and on very similar time scales. A few particles show a slow decay of the amplitude of the $r_{\rm G}(t)$

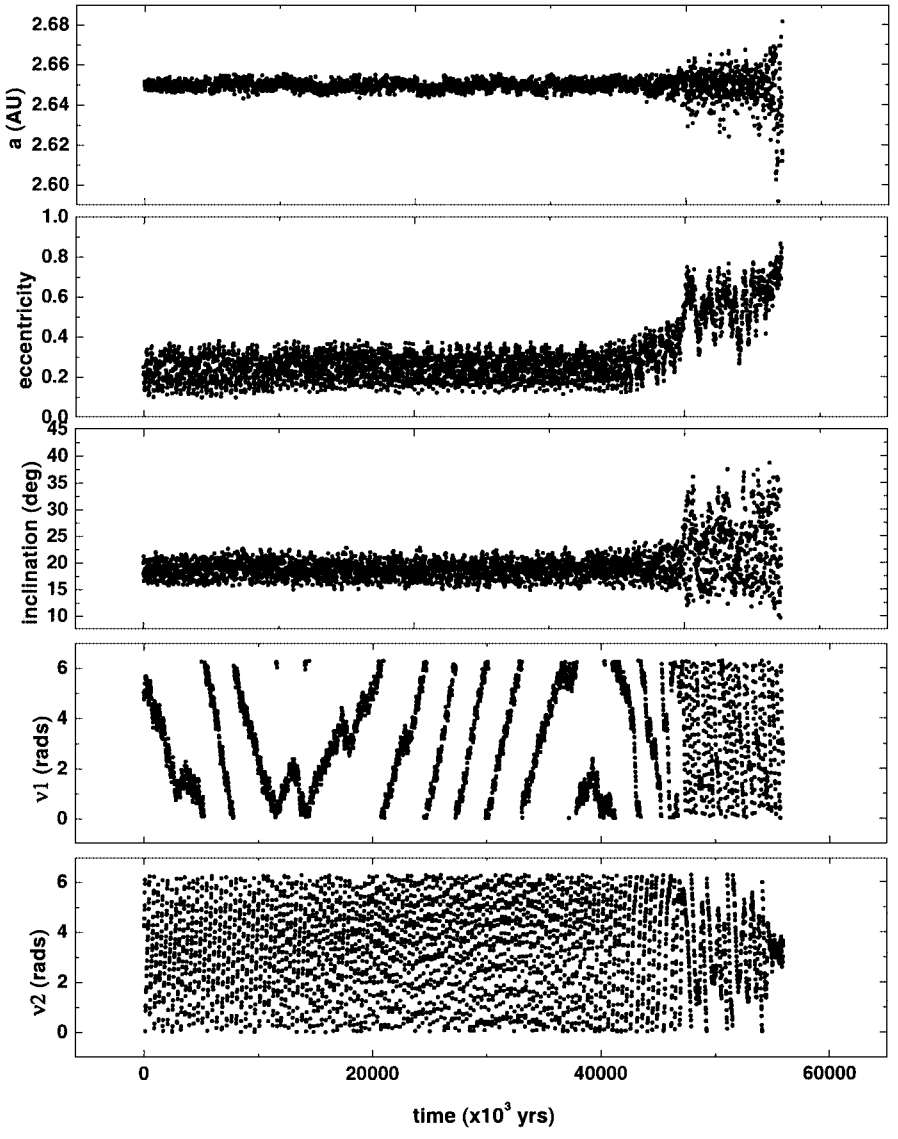

FIG. 14. The same as Fig. 13 but for the 11/4-escaping orbit starting at $e = 0.25$, $i = 20^\circ$. The critical arguments shown here are the ones corresponding to the $\langle \dot{\varpi} \rangle \approx g_5 + g_6 - g_8$ nonlinear resonance (noted by $\nu 1$) and the ν_6 resonance (noted by $\nu 2$; bottom). From the beginning the orbit is inside the $\nu 1$ resonance, which induces small-amplitude variations that cannot be easily identified from the osculating eccentricity time series. However, at the same time, it acts as a "mediator," injecting the particle into the ν_6 resonance after $t \approx 48$ Myr. After some librations inside the ν_6 resonance zone, the particle eventually becomes a Jupiter-crosser.

and $r_{\rm H}(t)$ time series, with the function resembling a "damped oscillator." A few exceptions to this general picture, for which all three $r(t)$s decay on a similar time scale but do not escape, are found among the high-eccentricity orbits of 13/6 particles, where three-body resonances, but also the 2/1 mean motion resonance with Jupiter, are probably playing an important role, as already mentioned.

The distribution of the autocorrelation times for L is shown in Fig. 16a. It is rather asymmetric, with a tail of ≈20% of the particles having $\tau_c > 2 \times 10^5$ years, but the median of the distribution is $\tau_c(L) = 20{,}000$ years, i.e., of the order of the Lyapunov time, $T_{\rm L}$. To calculate the value of τ_c we first calculated the "envelope" of $r(t)$ and then imposed an exponential fit on the resulting time series. For the other two actions, we had to use longer records (up to ≈50 Myr) for the calculation of $r(t)$. This, however, did not change the results much. The extremely slow decay of $r(t)$ results in an underestimate of τ_c, in general, for G and H. Thus the distributions shown in Figs. 16b and 16c are to be considered as indicative of the great difference in the time scale of correlation loss among the three actions. The medians of these distributions are $\tau_c(G) = 21$ Myr and $\tau_c(H) = 15$ Myr, respectively, i.e., of the order of $10^3 T_{\rm L}$.

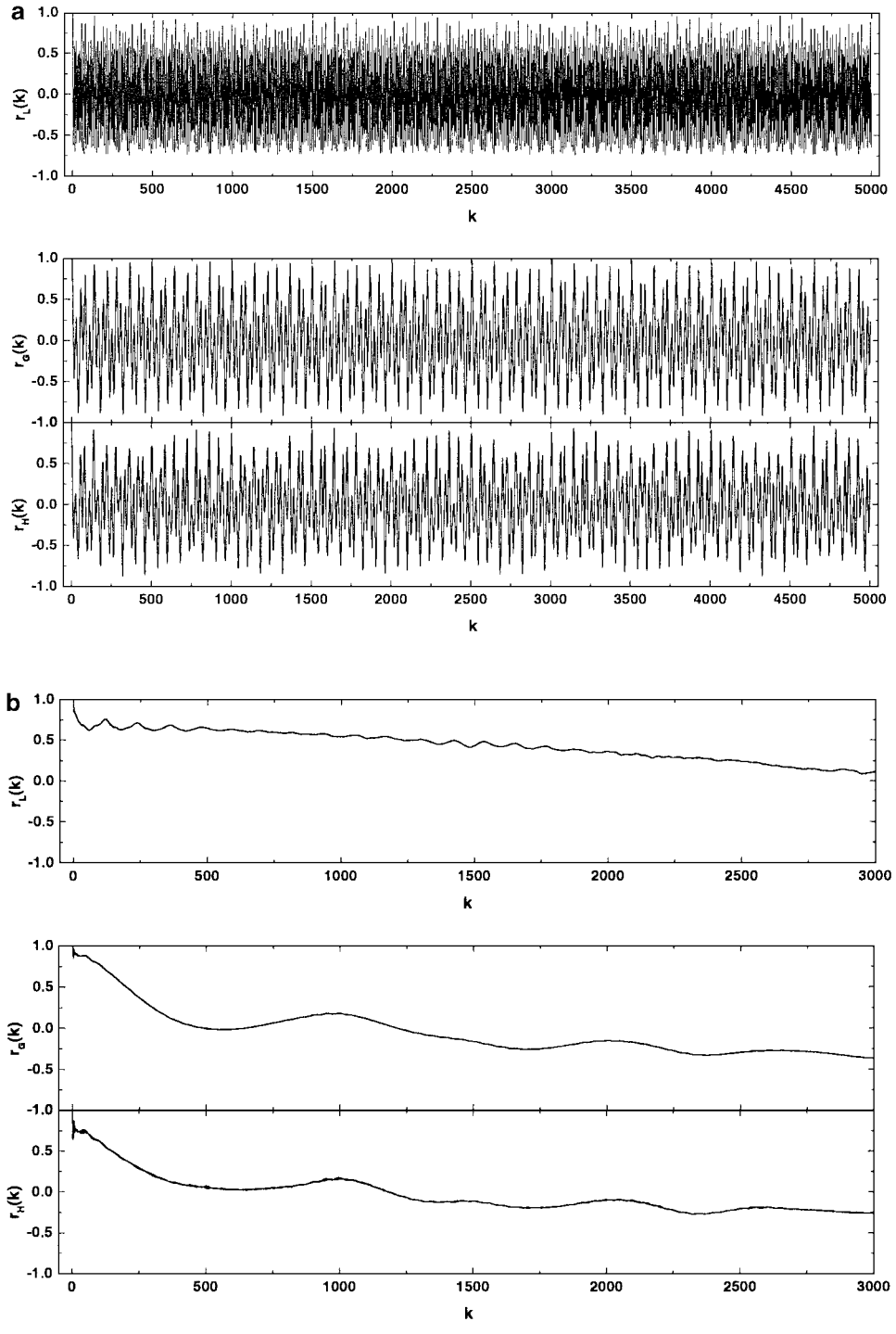

FIG. 15. The autocorrelation function $r(k)$ as a function of the time-lag k. The unit of time is $10^2 T_J$. Each three-panel figure shows $r(k)$ for the L, G, and H time series (top to bottom). (a) For a regular orbit all three functions vary quasi-periodically with time. (b) For the escapers, all three functions decay exponentially (on the average), with time, on a very similar time scale. (c) (d) The typical behavior of stable-chaotic orbits. $r_L(t)$ decays exponentially fast, while $r_G(t)$ and $r_H(t)$ vary quasi-periodically with time. (e) A few particles show a slow decay for $r_L(t)$—the other two functions are again quasi-periodic (f) The typical behavior for $r_L(t)$ accompanied by a slow decay of $r_G(t)$ and $r_H(t)$, which retain a strong quasi-periodic component, resembling the amplitude of oscillation of damped harmonic motion.

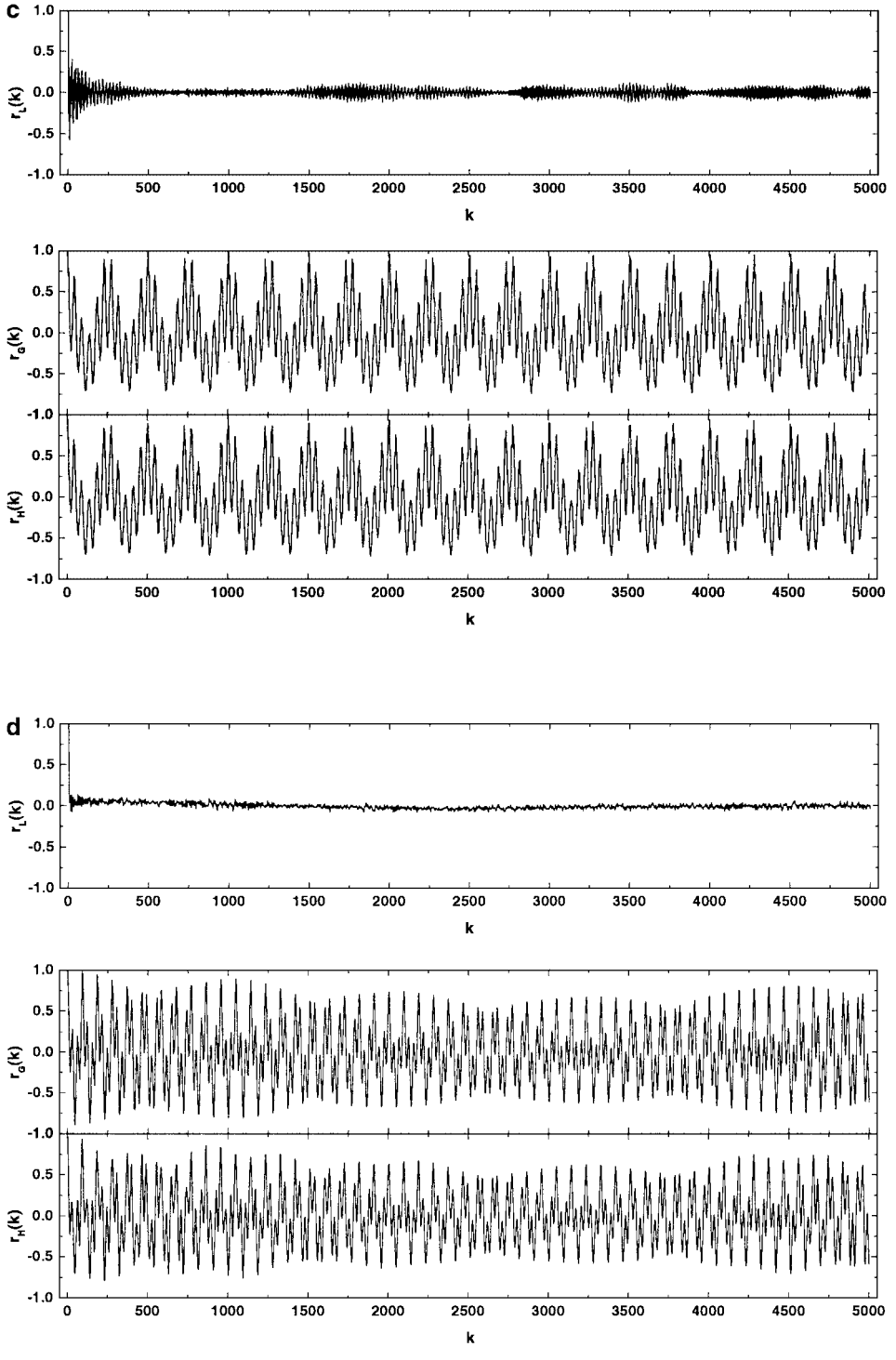

FIG. 15—*Continued*

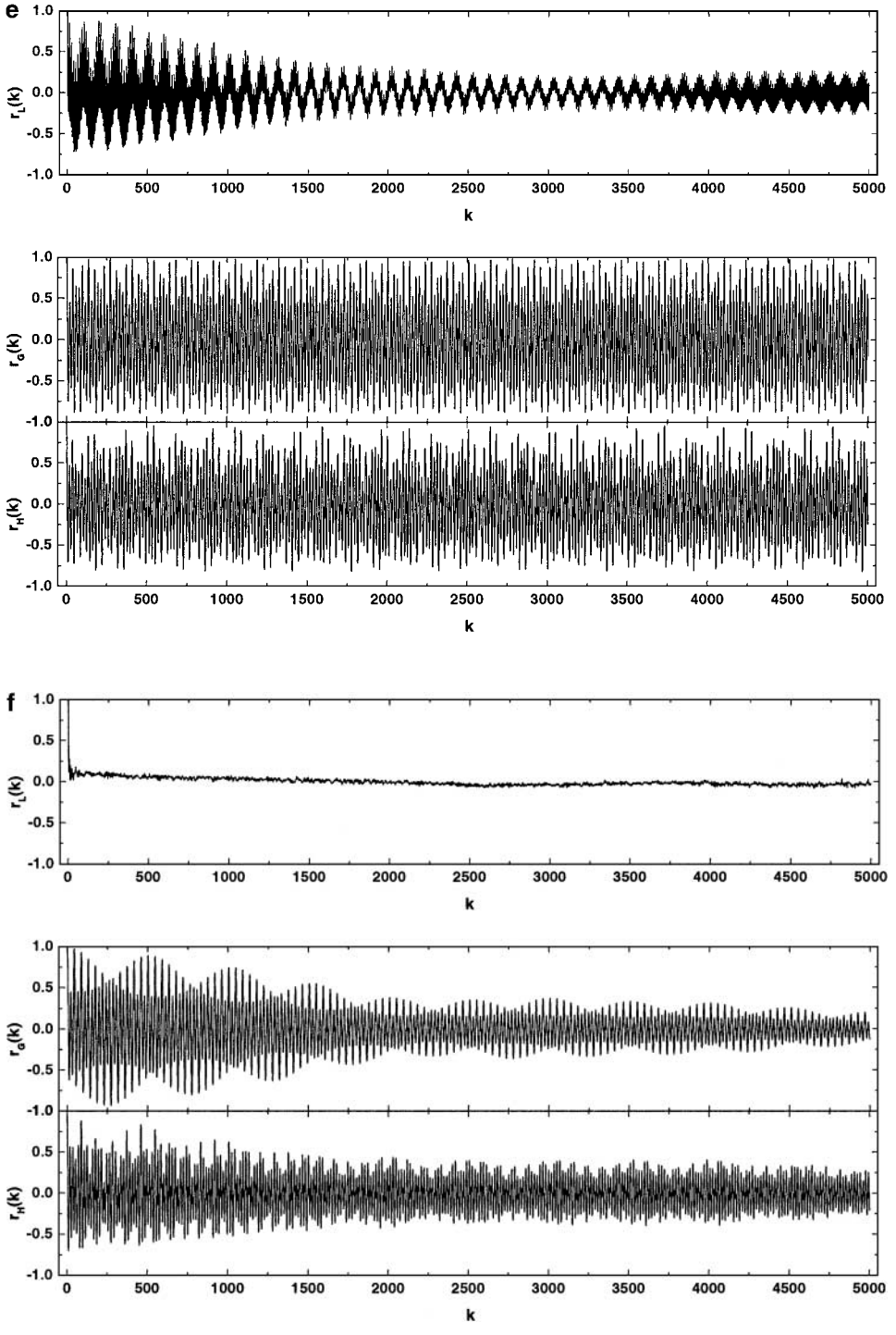

FIG. 15—*Continued*

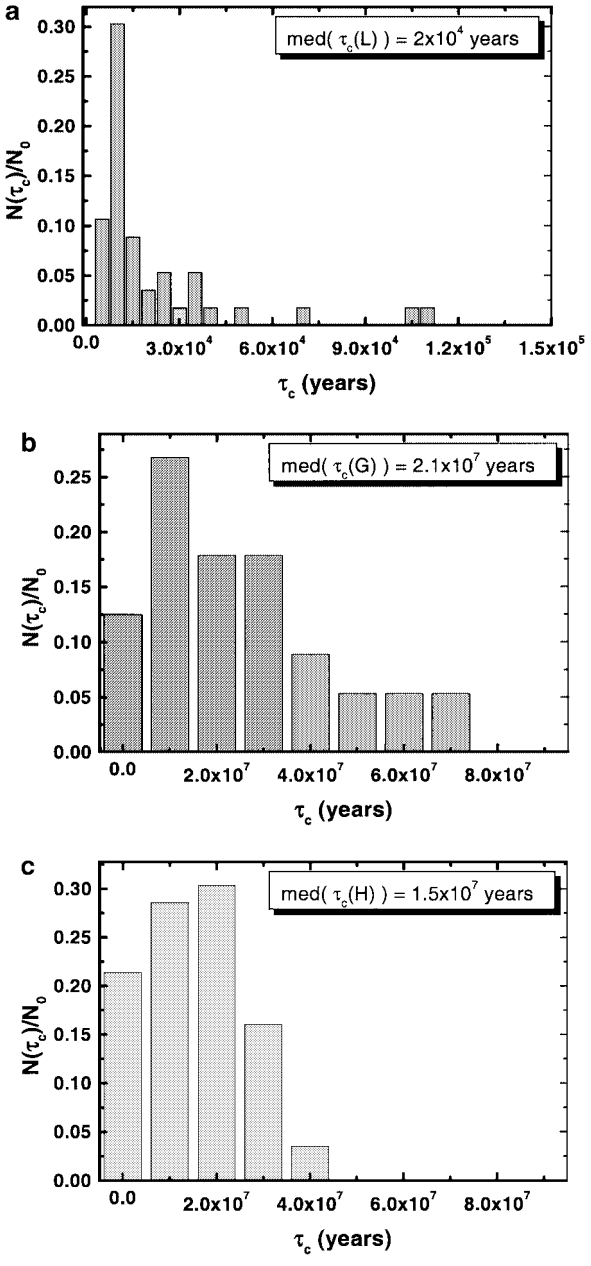

FIG. 16. The distribution of autocorrelation times for the (a) $L = \sqrt{a}$, (b) $G = L\sqrt{1-e^2}$, and (c) $H = G\cos i$ time series. The median time for L is of the order of $T_{\rm L}$, while for the other two actions the median time is of the order of $10^3 T_{\rm L}$.

5. DISCUSSION AND CONCLUSIONS

In this paper we continued our work on the phenomenon of stable chaos, which we began in Paper I by studying the motion of (522) Helga and the associated 12/7 jovian resonance. The conclusion of our previous work was that Helga's unusual motion is ultimately related to the absence of 12/7 resonant periodic orbits in the elliptic problem. This property produces an intriguing topology of the phase space near this resonance, which persists also under the influence of all outer planets. The *stickiness* hypothesis, which led us to that study, was not completely consistent with our numerical results and, in particular, the clear evidence of chaotic motion provided by the evolution of the critical argument. We argued that the notion of stickiness should be extended to incorporate trajectories for which chaotic nature is evident from the behavior of σ but which are semiconfined in eccentricity and inclination, due to the "mechanism" described above, within narrow regions of the phase space. What is implied by the last sentence is that the orbit seems to be sticky around an object in phase space which has dimensionality lower than that of the energy manifold. One can imagine the picture in the context of an autonomus three-degrees-of-freedom Hamiltonian system, such as the averaged 3-D elliptic restricted problem. Motion seems to take place close to a 4-D submanifold, $\mathcal{M}$, of the 5-D energy manifold, with $\mathcal{M}$ being the Cartesian product of a 2-torus with an annulus, $\mathcal{M} = \mathbf{T}^{(2)} \otimes \{\mathbf{S}^1 \otimes \mathbf{\Delta}\}$, $\mathbf{\Delta} \subset \mathbf{R}$. The radii of the 2-torus are related to the proper values of e and i, for which the motion is *stable*, while the *chaos* is evident in the third action (i.e., the semi-major axis), which is bounded inside the annulus by the resonance condition.

The study of resonant periodic orbits for the 11/4, 18/7, 13/6, and 22/9 resonances, in the present paper, showed that the same property holds for these cases also. Moreover, the numerical results showed that escape due to these resonances does not occur, at least for times of the order of 120 Myr, even when all giant planets are taken into account. Thus, we can conclude that the particular structure of the phase space, i.e., the absence of resonant periodic orbits, can lead to semiconfinement of chaotic orbits for times exceeding the Lyapunov time by many orders of magnitude. Compared to other resonances, where strong instability appears, as is the case with the 3/1 and 2/1 resonances, we could say that the topology of the phase space in these latter two resonances is very different from that of the 11/4, 18/7, 13/6, and 22/9 resonances that we consider in this paper. The reason is that in the 3/1 and 2/1 cases unstable periodic orbits exist both in the elliptic problem and in the 3-D problem. In a sense, the topology of the phase space, in the resonances studied here, looks more like the topology far from a resonance, rather than the typical resonant topology in places where gaps in the distribution of asteroids appear. This is true for a three-body model. However, in the vicinity of the 11/4 resonance ($a \simeq 2.65$ AU) and for $i \sim 20^\circ$ the evolution of asteroids is strongly influenced by a number of pericentric secular resonances, most notably the ν_6 resonance, which can enhance chaotic diffusion in the space of proper elements and lead to escape from the main belt. Indications for the action of three-body mean motion resonances were also found, especially close to the 13/6 resonance ($a \sim 3.1$ AU).

The phenomenology of stable chaos seems to be common among all jovian resonances that share the property of noncontinuation of resonant periodic orbits. The basic features of this

type of motion are:

- small values of T_L, typically in the range 10^3–5×10^4 years,
- evident chaotic evolution of the critical angles, σ,
- stable mean elements for times $>10^3 T_L$, and
- a characteristic spectrum of autocorrelation times, τ_cs, for the action time series.

The last feature, which was first noted in Paper I, means that there exists a striking difference between the values of the autocorrelation time for the action conjugate to σ (i.e., the semi-major axis), which is of the order of T_L, and the corresponding τ_c values for the actions that represent secular motion (i.e., proper eccentricity and inclination), which may be longer than $10^3 T_L$. This implies that the chaotic nature of an orbit in the vicinity of such a "flawed" resonance is not reflected in its secular evolution, at least for some set of initial conditions. This can be understood not only by the small variations in the amplitude of oscillations in e and i but also by the inability of the resonance to modify significantly the associated secular frequencies, $\dot{\varpi}$ and $\dot{\Omega}$, which is the reason for the strong quasi-periodic component of $r(t)$.

The chaos observed in these resonances should be attributed to the overlap among the terms of each resonance multiplet. Even if resonance-overlap is exhaustive, the characteristic diffusion time for a chaotic orbit may be comparable to the age of the Solar System, according to Murray and Holman (1997), so that the terminology *stable chaos* results in a natural way. However, assuming a "random-walk" in e associated to the chaotic wandering of a may not be safe, at least for all sets of initial conditions. The orbits which we characterize as "stable-chaotic" have autocorrelation functions for G and H that do not decay exponentially with time. This is clearly not a typical random walk. One would expect that, in the resonance-overlap regime, the eccentricity has a typical irregular evolution (possibly of very small amplitude), whose uncorrelated "jumps" are visible on a time scale comparable to the Lyapunov time. This is *not* the case for our stable-chaotic orbits. We believe, therefore, that what we describe as "stable-chaos," which is a term characterizing the exact same behavior as that of the asteroid (522) Helga (see Paper I), is not the same type of motion as the one described by Murray and Holman (1997), which can be a very "slow chaos" indeed. In fact, we believe, but this is simply a conjecture, that the phenomenon we describe appears only in models with more than three degrees of freedom: there seems to be a set of initial conditions for which a second, local, integral exists and this results in a nearly quasi-periodic evolution of the actions, which is what we observe. This is what we described above as a case of stickiness around an object of dimensionality lower than that of the energy manifold.

The ability of a mean motion resonance to remove asteroids from its neighborhood, within a reasonably short time scale (<100 Myr), depends critically on whether the main family of resonant periodic orbits of the circular problem is continued to the elliptic problem and the 3-D problem. This remark can help in explaining, partly, the abundance of real-life resonant asteroids following chaotic orbits; these objects should be regarded as cases of stable chaos, since they are permanent members of the main belt. Also, it can add a small piece to the puzzle concerning the formation of gaps in the asteroid belt and, in particular, in explaining why only a small number of gaps, close to low-order resonances, exist in the main belt, while numerical studies show that strong chaos, in terms of Lyapunov exponents, is prominent throughout the belt. Recall that the main Kirkwood gaps are located near the 2/1, 3/1, 4/1, and 5/2 mean motion resonances, all of which are known to posses the property of continuation of the main family of resonant periodic orbits for more than one value of the asteroid's eccentricity (see Hadjidemetriou 1993b and also Section 2 in this paper for the 5/2 case). Thus, if only a small number of low-order resonances carry periodic orbits that are continued in the elliptic problem, these would be the ones having the ability to "sculpt" a gap inside the main belt, in the first place. Of course, it is known that the depletion of the main Kirkwood gaps cannot be explained in the framework of the elliptic restricted problem, and other mechanisms (primarily the secular resonances) have to be accounted for. In the rest of medium-to-high-order mean motion resonances, semiconfined chaotic motion (i.e., stable chaos) can exist with characteristic diffusion times, most probably, greater than the age of our Solar System. A survey of these resonances is currently under way, with very encouraging initial results.

ACKNOWLEDGMENTS

We thank Alessandro Morbidelli, Matt Holman, and an anonymous referee for their constructive criticism, which significantly improved the presentation of our work. K. Tsiganis wishes to acknowledge financial support from the State Scholarship Foundation of Greece (IKY).

REFERENCES

Bretagnon, P. 1974. Termes à longues périodes dans le système solaire. *Astron. Astrophys.* **30**, 141–154.

Dvorak, R., and K. Tsiganis 2000. Why do Trojan ASCs (not) escape? *Celest. Mech. Dynam. Astron.* **78**, 125–136.

Farinella, P., Ch. Froeschlé, C. Froeschlé, R. Gonczi, G. Hahn, A. Morbidelli, and G. B. Valsecchi 1994. Asteroids falling onto the Sun. *Nature* **371**, 315–317.

Hadjidemetriou, J. D. 1993a. Asteroid motion near the 3 : 1 resonance. *Celest. Mech. Dynam. Astron.* **56**, 563–599.

Hadjidemetriou, J. D. 1993b. Resonant motion in the restricted three-body problem. *Celest. Mech. Dynam. Astron.* **56**, 201–219.

Holman, M., and N. Murray 1996. Chaos in high-order mean motion resonances in the outer asteroid belt. *Astron. J.* **112**, 1278–1293.

Klafke, J. C., S. Ferraz-Mello, and T. Michtchenko 1992. Very-high-eccentricity librations at some higher-order resonances. *IAU Symposium* **152**, 153–158.

Knežević, Z., A. Milani, P. Farinella, Ch. Froeschlé, and C. Froeschlé 1991. Secular resonances from 2 to 50 AU. *Icarus* **93**, 316–330.

Laskar, J. 1990. The chaotic motion of the Solar System: A numerical estimate of the size of the chaotic zones. *Icarus* **88**, 266–291.

Levison, H. F., and M. J. Duncan 1994. The long-term dynamical behavior of short-period comets. *Icarus* **108**, 18–36.

Milani, A., and A. M. Nobili 1992. An example of stable chaos in the Solar System. *Nature* **357**, 569–571.

Milani, A., A. Nobili, and Z. Knežević 1997. Stable chaos in the asteroid belt. *Icarus* **125**, 13–31.

Moons, M., and A. Morbidelli 1995. Secular resonances inside mean-motion commensurabilities: The 4/1, 3/1, 5/2 and 7/3 cases. *Icarus* **114**, 33–50.

Morbidelli, A., and D. Nezvorný 1999. Numerous weak resonances drive asteroids toward terrestrial planets orbits. *Icarus* **139**, 295–308.

Murison, M., M. Lecar, and F. Franklin 1994. Chaotic motion in the outer belt and its relation to the age of the Solar System. *Astron. J.* **108**, 2323–2329.

Murray, N., and M. Holman 1997. Diffusive chaos in the outer asteroid belt. *Astron. J.* **114**, 1246–1259.

Murray, N., M. Holman, and M. Potter 1998. On the origin of chaos in the asteroid belt. *Astron. J.* **116**, 2583–2589.

Nautical Almanac Office, U.S. Naval Observatory 2000. *The Astronomical Almanac*, U.S. Government Printing Office, Section E3.

Nesvorný, D., and A. Morbidelli 1998. Three-body mean motion resonances and the chaotic structure of the asteroid belt. *Astron. J* **116**, 3029–3037.

Nobili, A. M., A. Milani, and M. Carpino 1989. Fundamental frequencies and small divisors in the orbits of the outer planets. *Astron. Astrophys.* **210**, 313–336.

Šidlichovský, M. 1999. On stable chaos in the asteroid belt. *Celest. Mech. Dynam. Astron.* **73**, 77–86.

Tsiganis, K., H. Varvoglis, and J. D. Hadjidemetriou 2000. Stable chaos in the 12 : 7 mean motion resonance and its relation to the stickiness effect. *Icarus* **146**, 240–252.

Varvoglis, H., and A. Anastasiadis 1996. Transport in Hamiltonian systems and its relationship to the Lyapunov time. *Astron. J.* **111**, 1718–1720.

Wisdom, J. 1983. Chaotic behavior and the origin of the 3/1 Kirkwood gap. *Icarus* **56**, 51–74.

Wisdom, J., and M. Holman 1991. Symplectic maps for the *n*-body problem. *Astron. J.* **102**, 1528–1538.